NTNU

Norwegian University of
Science and Technology

# Experimental Investigation of Osmosis as a Mechanism for Low-Salinity EOR

Erik N. Pollen

Petroleum Geoscience and Engineering
Submission date: June 2017
Supervisor: Carl Fredrik Berg, IGP
Co-supervisor: Kristian Sandengen, Statoil ASA

Norwegian University of Science and Technology
Department of Geoscience and Petroleum

# Summary

The topic of this thesis is an experimental investigation of osmosis as a mechanism for low-salinity enhanced oil recovery by evaluation of the effect of surface-to-volume ratio on oil recovery. Increased oil recovery due to osmosis is expected to have a stronger correlation to the surface-to-volume ratio than other low-salinity EOR mechanisms.

Low-salinity spontaneous imbibition tests were performed on oil-wet Bentheimer sandstone samples with varying surface-to-volume ratios. Fluids and core samples were chosen to promote osmosis-induced connate water expansion while impeding the effects of other proposed low-salinity mechanisms.

The experiment was performed twice, the first at elevated temperatures and second at ambient temperature. The experiment at elevated temperature resulted in low values of increased oil production by low-salinity spontaneous imbibition. The low response is believed to be caused by thermal effects from repeated heating and cooling of the samples. The experiment at ambient temperature resulted in increased oil production values of $8 - 22\%$ of pore volume. No clear correlation was found between increased oil recovery and the surface-to-volume ratio. A correlation was, however, seen between increased oil production and pore volume.

The results of the experiment were unsuccessful in determining the relative importance of osmosis in either small scale low-salinity experimental results or larger scale low-salinity EOR. The results of the experiment do not reject osmosis as a mechanism for low-salinity EOR. Two possible explanations of how increased oil production relates to the pore volume are presented.

# Sammendrag

I denne oppgaven undersøkes osmose som en mulig mekanisme for økt oljeutvinning ved bruk av vann med lavt saltinnhold. Dette gjøres ved å undersøke forholdet mellom økt oljeutvinning og overflate-volum-forholdet. Grunnlaget for undersøkelsen er at osmose forventes å ha en sterkere korrelasjon til overflate-volum-forholdet enn andre EOR mekanismer for økt oljeutvinning ved bruk av vann med lavt saltinnhold

Forsøk med spontan imbibering ble utført på oljefuktende kjerneprøver med varierende overflate-volum-forhold. Forsøket ble designet for å fremme effekter osmose og samtidig redusere virkningene av andre foreslåtte mekanismer.

Forsøket ble utført to ganger, en gang ved høy temperaturer og en gang ved romtemperatur. Forsøket som ble gjennomført ved høy temperatur resulterte i generell lav oljeutvinning. Den lave responsen antas å være forårsaket av termiske effekter fra gjentatt oppvarming og avkjøling av prøvene. Forsøket som ble gjennomført ved romtemperatur resulterte i oljeutvinning på $8-22\%$ av porevolumet. Resultatene viser ingen tydelig korrelasjon mellom oljeutvinning og overflate-til-volumforholdet. En korrelasjon ble derimot sett mellom oljeutvinning og porevolumet.

Resultatene av forsøket klarte ikke å evaluere betydningen av osmose i eksperimenter eller i EOR-anvendelser med vann med lavt saltinnhold. Resultatene av forsøket avviser ikke osmose som mekanisme i "low-salinity EOR". To mulige forklaringer om hvordan økt oljeutvinning relaterer til porevolumet har blitt presentert.

# Acknowledgements

This thesis is written as a part of my Master's degree in Petroleum Engineering with specialization in Reservoir Engineering and Petrophysics at the Norwegian University of Science and Technology (NTNU).

Many people have been involved in this work and I would like to express my gratitude to those who have contributed. First of all, I would like to thank my supervisor, Associate Professor Carl Fredrik Berg (NTNU), for providing me with an interesting topic, for frequently following up my work and for sharing his knowledge. Second, I would like to thank my co-supervision, Dr. Kristian Sandengen (Statoil), for sharing his knowledge and experience related to both the topic and laboratory procedures, and for providing core samples for the experiment. I would also like to thank Roger Overå (NTNU) for excellent assistance in the laboratory.

Trondheim, 26.06.2017

# Table of Contents

# List of Tables

# List of Figures

# Nomenclature

| | | |
|---|---|---|
| $\Delta V_{HS,oil}$ | = | oil production using high-salinity water [$cm^3$] |
| $\Delta V_{LS,oil}$ | = | increased oil production using low-salinity water [$cm^3$] |
| $\Delta V_{HS,i}$ | = | increased oil production by high-salinity spontaneous imbibition for sample $i = A, B, C, D$ [$cm^3$] |
| $\Delta V_{LS,i}$ | = | increased oil production by low-salinity spontaneous imbibition for sample $i = A, B, C, D$ [$cm^3$] |
| $\Delta v_{osmosis}$ | = | increased oil production by osmosis per surface area [$cm$] |
| $\Delta v_{surface}$ | = | increased oil production per surface area [$cm$] |
| $\Delta v_{volume}$ | = | increased oil production per pore volume [-] |
| $\phi_e$ | = | effective porosity [-] |
| $\mu$ | = | viscosity [$Pa \cdot s$] |
| $\tau$ | = | tortuosity [-] |

| | | |
|---|---|---|
| $A$ | = | surface area [$cm^3$] |
| $A(x)$ | = | cross-sectional area at position x [$m^2$] |
| $a_{brine}$ | = | water activity in brine [-] |
| $C$ | = | constriction factor [-] |
| $c$ | = | concentration [$\frac{mol}{m^3}$] |
| $c_{brine}$ | = | water-in-oil solubility in oil in equilibrium with brine [$mol$] |
| $c_w$ | = | water-in-oil solubility [$mol$] |
| $c_0$ | = | water-in-oil solubility in oil in equilibrium with pure water [$mol$] |
| $D$ | = | diffusion coefficient [$\frac{m^2}{s}$] |
| $D_e$ | = | effective diffusion coefficient [$\frac{m^2}{s}$] |
| $D_0$ | = | bulk diffusion coefficient [$\frac{m^2}{s}$] |
| $d_j$ | = | diameter of slice $i$ [m] |
| $\mathbf{J}$ | = | diffusion flux vector [$\frac{mol}{m^2 \cdot s}$] |
| $k_B$ | = | Boltzmann's constant [$\frac{J}{K}$] |
| $L$ | = | core length [$m$] |
| $l$ | = | flow path length [$m$] |
| $r$ | = | droplet radius [$m$] |
| $s$ | = | straight-line length [$m$] |
| $S_{or}$ | = | residual oil saturation [-] |
| $S_w$ | = | water saturation [-] |
| $S_{wi}$ | = | initial water saturation [-] |
| $S_{wir}$ | = | irreducible water saturation [-] |
| $T$ | = | temperature [$K$] |
| $t$ | = | time [$s$] |
| $V_{bulk}$ | = | bulk volume [$cm^3$] |
| $V_{grain}$ | = | grain volume [$cm^3$] |
| $V_{pore}$ | = | pore volume [$cm^3$] |
| $V_1$ | = | volume of gas in empty chamber [$cm^3$] |
| $V_2$ | = | volume of gas in chamber containing core [$cm^3$] |
| $z$ | = | oil membrane thickness [$m$] |
| $z_j$ | = | height of slice $i$ [m] |

Chapter 1

# Introduction

Low-salinity waterflooding is an enhanced oil recovery (EOR) technique in which reduced salinity water is injected into a reservoir to achieved additional oil recovery compared to conventional waterflooding. Despite increasing interest in low-salinity EOR, the technique is not properly understood and a consistent mechanistic framework has not yet emerged. Several low-salinity mechanisms have been proposed and it has been suggested that either there are multiple mechanisms underlying the low-salinity effect or the primary mechanism has not yet been identified [1, 2].

Sandengen and Arntzen (2013) recently proposed osmosis as a mechanism for low-salinity EOR. It was hypothesized that oil acts as a semi-permeable membrane that passes water but not ions, thereby causing connate water expansion and relocation of oil. Previous investigations of osmosis as an underlying mechanism have consisted of visualization experiments. In these experiments, water transport and oil movement under influence of osmotic gradients have been observed.

The topic of this thesis is an experimental investigation of osmosis as a mechanism for low-salinity enhanced oil recovery by evaluation of the effect of surface-to-volume ratio on oil recovery. Increased oil recovery due to osmosis is expected to have a stronger correlation to the surface-to-volume ratio than other proposed mechanisms for low-salinity EOR. By comparing oil recovery to surface-to-volume ratio, we will try to obtain a qualitative understanding of the relative importance of osmosis on both experimental results and larger scale low-salinity EOR.

Chapter 2

# Background

In this section we will introduce the development of low-salinity as an EOR method, how the performance of low-salinity EOR can be quantified and introduce the proposed low-salinity mechanisms, before reviewing previous findings on osmosis as a low-salinity mechanism.

## 2.1 Low-Salinity Enhanced Oil Recovery

Low-salinity enhanced oil recovery is a recovery technique in which reduced salinity water is injected into a reservoir to achieved additional oil recovery compared to conventional waterflooding. Typically, increased oil recovery by low-salinity waterflooding has been reported for water salinities less than $5,000\ ppm$ [1, 3].

The effects of brine composition on wettability and oil recovery were first reported by Jadhunandan (1990) who used brine composition to alter the wettability of a crude oil/brine/rock system in an effort to determine the relationship between wetting conditions and oil recovery [4].

Later, Tang and Morrow (1997) reported enhanced oil recovery by low-salinity waterflooding [5]. The results were based on an extensive laboratory study of how oil recovery in spontaneous imbibition and waterflooding experiments were affected by systematic variation in both connate and invading water salinity. The experiments were performed on Berea sandstone core samples saturated with crude oil and water at initial water saturation ($S_{wi}$), representing the field fluid configuration at the start of oil production.

Tang and Morrow (1997) studied the effect of water salinity in three parts: Oil recovery using identical brines for connate and invading water (Figures 2.1); oil recovery using high-salinity connate water while varying the invading water salinity (Figure 2.2); and oil recovery using high-salinity invading water while varying the connate water salinity

(Figure 2.3). For the oil/brine/rock system studied, there was a clear trend of increasing oil recovery in both spontaneous imbibition and waterflooding experiments with decreasing salinity in either the connate water, the invading water or both.

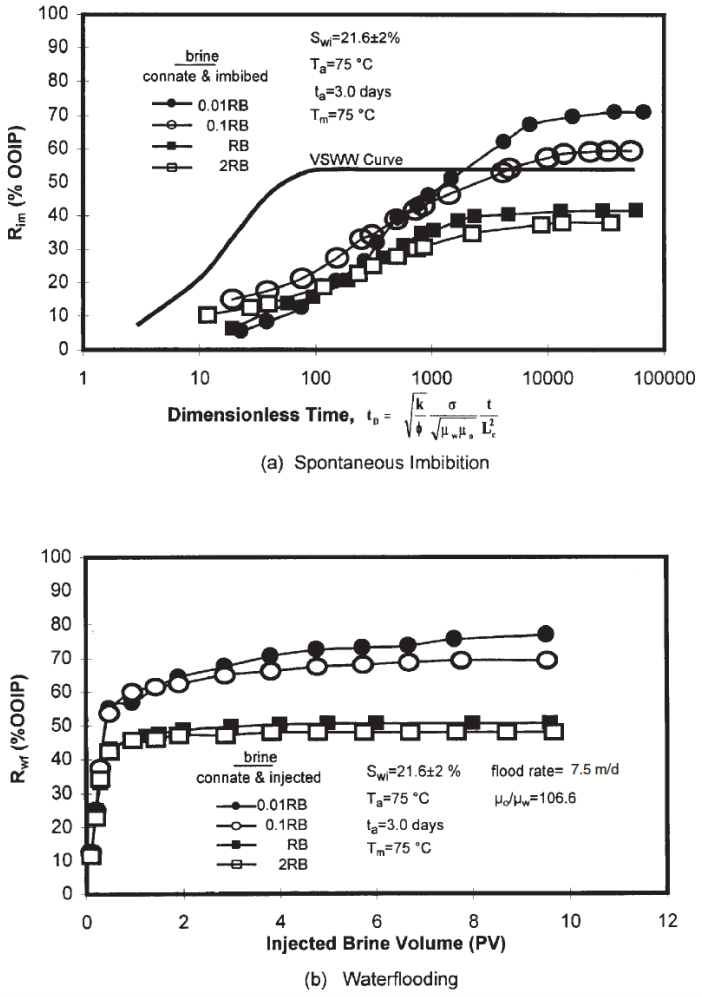


**Figure 2.1:** (a) Oil recovery vs. dimensionless time for spontaneous imbibition experiments and (b) oil recovery vs. injected pore volumes (PV) for waterflooding experiments. The salinity of connate and imbibing/injection water are equal and varied simultaneously. $0.1RB$ indicates reservoir brine (RB) that has been diluted ten times. The VSWW (very strongly water wet) curve is used as reference for the spontaneous imbibition experiments. [5, 6]

In addition to laboratory test, enhanced oil recovery by low-salinity waterflooding has also been reported in field tests. Webb et al. (2004) reported $25 - 50\%$ reduction in residual oil saturation ($S_{or}$) near the wellbore when changing from high-salinity to low-

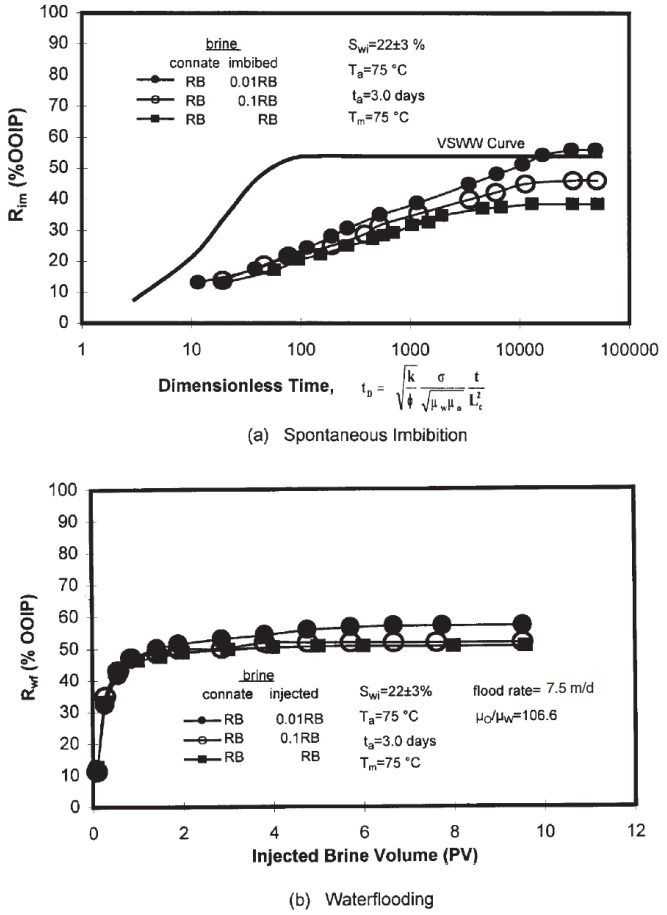


**Figure 2.2:** (a) Oil recovery vs. dimensionless time for spontaneous imbibition experiments and (b) oil recovery vs. injected PV for waterflooding experiments. The experiments use fixed high-salinity connate water and invading water of varying salinity. [5]

salinity waterflooding based on logging before and after chaning the injection water [7]. McGuire et al. (2005) reported a significant reduction in residual oil saturation in the near-well region based on results from a single well chemical tracer tests [3]. Lager et al. (2008) reported successful inter-well low-salinity trial based on observations of a water cut reduction coinciding with a sudden change in produced water chemistry [8]. Seccombe et al. (2010) reported recovery of residual oil at inter-well scale as a decrease in water cut coincided with the breakthrough of reduced salinity water after changing from high-salinity to low-salinity waterflooding [9].

There are several reports of positive effects of low-salinity waterflooding from both laboratory and field tests; however, non-positive results are also widely reported. One of these is Skrettingland et al. (2010) who reported low or no effect of low-salinity waterflooding

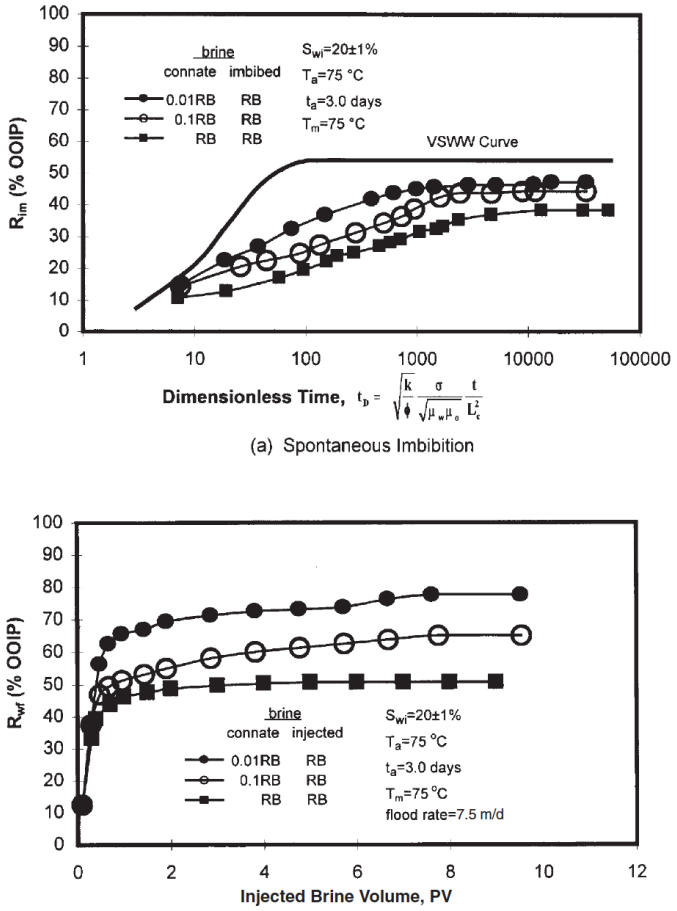


**Figure 2.3:** (a) Oil recovery vs. dimensionless time for spontaneous imbibition experiments and (b) Oil recovery vs. injected PV for waterflooding experiments. The experiments use connate water of varying salinity and fixed high-salinity invading water. [5]

during evaluation of low-salinity EOR for the Snorre field, in the North Sea. His conclusion was based on results from both core flooding tests and single well chemical tracer tests [10].

It has been difficult to predict the behavior of low-salinity waterflooding and several requirements have been suggested in order achieve increased oil recovery by low-salinity waterflooding. Some of these requirements are the presence of connate water, significant clay amounts and crude oil [11]. These requirements are, however, subject to debate as there are many examples of experimental results contradicting the proposed requirements.

### 2.1.1 Measuring the Effect of Low-Salinity EOR

Low-salinity effect (LSE) is a measure of the performance of low-salinity waterflooding compared to conventional high-salinity waterflooding. How the low-salinity effect is quantified depends on when low-salinity waterflooding is applied to system.

As a secondary recovery technique, where low-salinity water is injected from the start of production, the low-salinity effect is quantified as the additional oil recovered compared to if conventional high-salinity waterflooding had been performed (see Figure 2.4). This requires two sets of data, oil recovery during low-salinity waterflooding and oil recovery during conventional waterflooding. For field cases, recording the low-salinity effect is, therefore, challenging because only one data set may be obtained. In laboratory studies, however, use of multiple core samples or repeating coreflooding experiments on the same core enable us to collect multiple data sets. However, this approach may give inaccurate results because no cores are exactly alike and re-establishing equal initial saturation conditions is difficult.

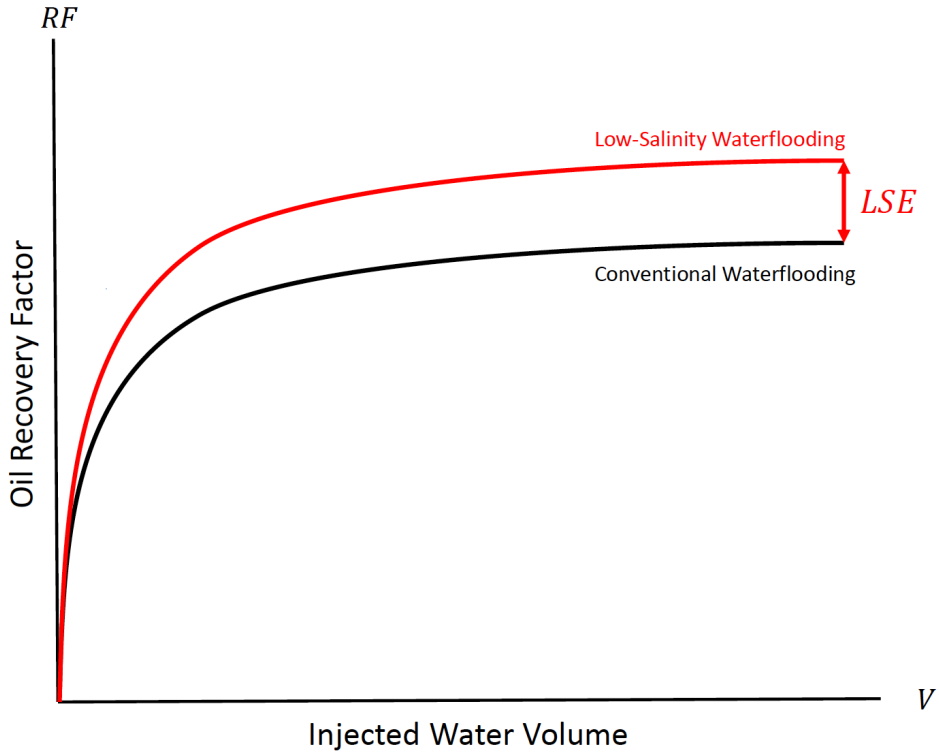


**Figure 2.4:** Illustration of the low-salinity effect (LSE) in secondary recovery mode.

As a tertiary recovery technique, where low-salinity waterflooding is initiated following conventional waterflooding and the reservoir has reached near residual oil saturation ($S_{or}$), the low-salinity effect can be quantified as the additional oil recovered after switching to

low-salinity waterflooding (see Figure 2.5). In laboratory test, it is recommended to establish a base case where the procedure of switching water phase is conducted, without changing salinity. This may rule out effects like pressure waves causing increase oil recovery.

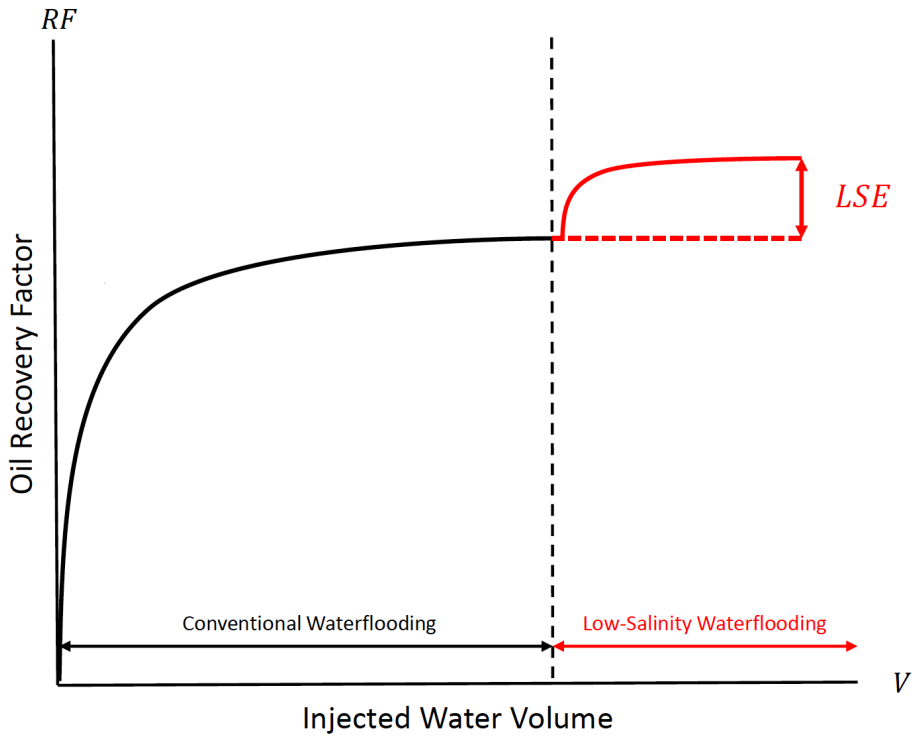


**Figure 2.5:** Illustration of the low-salinity effect (LSE) in tertiary recovery mode.

One important difference between the low-salinity effect from secondary and tertiary recovery modes is the range of the effect. The low-salinity effect for secondary recovery can be positive, negative or zero. The low-salinity effect for tertiary recovery however is by nature non-negative. This is because the worst case scenario for tertiary low-salinity waterflooding is no increase in oil recovery.

There are no typical values for the low-salinity effect. The recorded effects from laboratory experiments range from no effect to incremental and high low-salinity effect. Laboratory experiments do, however, indicate that performing low-salinity waterflooding in secondary mode generally yields higher low-salinity effects than in tertiary mode. [1]

### 2.1.2 Field Applications of Low-Salinity EOR

Despite extensive research on low-salinity EOR and at least one pilot project on a injector-producer pair, there are still no full-field applications of the technology. One of the factors believed to cause the slow take-up of low-salinity waterflooding is that low-salinity it enhances but does not enable, projects economics [12]. BP (British Petroleum) announced that the Clair Ridge field, a tight and fractured sandstone reservoir, is expected to be the first full-field application of low-salinity EOR [13]. First oil from the field is expected in 2018 and low-salinity waterflooding will be performed in secondary recovery mode, i.e. from the start of production [14, 15].

The main requirement to perform full-field low-salinity EOR is a large supply of low-salinity water. This can be achieved by manufacturing low-salinity water from high-salinity water. Large natural low-salinity water sources may also be evaluated as alternatives. There are several methods for large-scale manufacturing of low-salinity water, one of these technologies is membrane desalination by reverse osmosis. Some important considerations for the application of low-salinity EOR to offshore fields are the spatial and power limitations on an offshore production rig. Therefore, the additional required complexity of the injection system needs to be limited. Integration of membrane desalinization within a conventional waterflooding system design is a solution that is in line with these restrictions [12]. A schematic of an integrated system design is presented in Figure 2.6. Table 2.1 shows an example of the composition of input seawater and the desalinized water from a membrane desalination process.

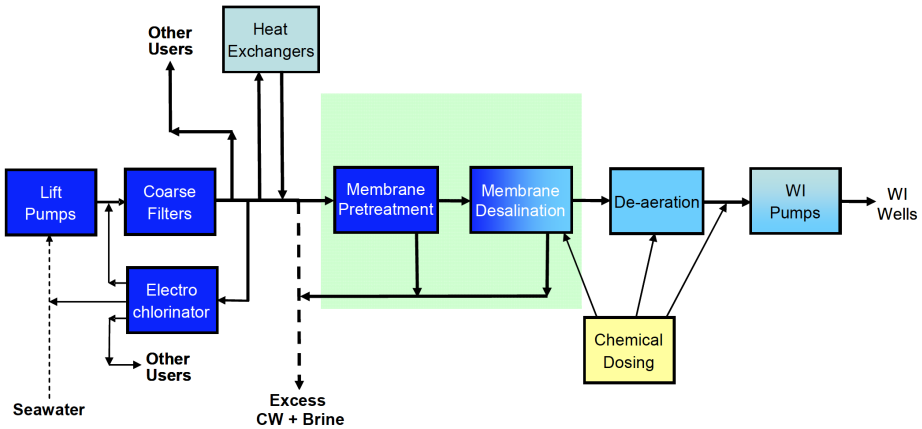


**Figure 2.6:** Schematic of integrated system design of membrane pre-filtration and membrane desalination in a conventional waterflooding module. The ”UF Membrane Pretreatment” and ”Membrane Desalination” units make up the additional required steps compared to a conventional waterflooding module. [12]

**Table 2.1:** Example of change in ionic composition by membrane desalination. Total dissolved solids (TDS) is typically used to describe salinity. [16]

| Ion | Seawater composition [ppm] | Permeate composition [ppm] |
|---|---|---|
| $Cl^-$ | 19,940 | 97.71 |
| $Na^+$ | 10,869 | 57.61 |
| $SO_4^{2-}$ | 2,722 | 1.36 |
| $Mg^{2+}$ | 1,314 | 1.64 |
| $Ca^{2+}$ | 422 | 0.53 |
| $K^+$ | 402 | 2.41 |
| $HCO_3^{2-}$ | 125 | 0.94 |
| $CO_3^-$ | 16 | 0.00 |
| $Br^{2+}$ | 71 | 0.53 |
| $Sr^{2+}$ | 8 | 0.01 |
| **TDS** | 35,889 | 167.74 |

In addition to the possibility of increased oil recovery, there are several other benefits of using low-salinity water related to chemical production issues. The most frequently mentioned benefits are related to the reduction of sulfate ($SO_4^{2-}$) in the injection water. By using low-salinity water there is a significantly reduced potential for scaling in production tubing and reservoir plugging due to precipitation when sulfate mixes with barium ($Ba^{2+}$) or strontium ($Sr^{2+}$) present in the formation water. The risk of reservoir souring is also significantly reduced by reducing the injected sulfate, which acts as a source of sulfur that can be converted to hydrogen sulfide ($H_2S$) by sulfate-reducing bacteria. [16]

Despite concerns of clay swelling causing formation damage during low-salinity water-flooding, no cases of significant formation damage have been recorded during field tests. In fact, another benefit of using low-salinity water injection is maintained injectivity over time due to injection of high-quality filtered water, which may prevent plugging of the formation near the injectors. [16]

Based on holistic benefits such as increased oil recovery, improved maintainability of injectivity, and reduced risk of scaling and souring, it is apparent that use of low-salinity water may be beneficial with regard to both project economics and to health, safety and environment (HSE).

### 2.1.3 Low-Salinity Mechanisms in Sandstones

Several low-salinity mechanisms have been proposed and investigated, however, no individual mechanism has been identified to be the primary cause of the low-salinity effect. It has been suggested that either there are multiple mechanisms underlying the low-salinity effect or the primary mechanism has not yet been identified [2].

Figure 2.7 shows an overview of proposed low-salinity mechanisms and how they contribute to increased oil recovery. Note that this should not be considered as a complete overview. The following sections present some central mechanisms that have been suggested. Osmosis will not be presented here, but will be reviewed thoroughly in Section 2.2.

#### Fines Migration

It is known that changes in water salinity may affect the stability of clay in the formation. A decrease in water salinity may destabilize the formation clay causing dispersion of clay and silt sized particles into the fluid flow [11]. One of the earliest proposed low-salinity mechanism was fines migration. Fines migration is typically used as a collective term of enhanced oil recovery mechanisms caused by destabilization and release of fine solids.

Tang et al. (1999) suggested that presence of potentially mobile fines is required for oil recovery to be sensitive to salinity during waterflooding and spontaneous imbibition experiments. Through their experiments, it was observed that Berea sandstone cores that had been fired and acidized, to stabilize mobile fines and remove metal oxides, were insensitive to brine salinity. Cores that had been subject to extensive flooding were also reported to be insensitive to brine salinity. It was also observed that that Bentheimer and Clashach sandstone cores, which are known to have low clay-content compared to Berea sandstone, and therefore less potentially mobile fines, had significantly reduced sensitivity to brine salinity. Based on these observations Tang et al. (1999) concluded that low-salinity water improved oil recovery by producing mixed-wet fines with attached crude oil, thus mobilizing residual oil. [17, 18]

In addition to the production of oil attached to oil-wet solids, it has been suggested that dispersed solid particles may become lodged in pore throats along high permeability flow paths, restricting and redirecting the flow into less permeable flow paths. This microscopic flow diversion is proposed to improve the sweep efficiency at the pore scale. [11]

#### Effects of Increased pH

Based on observed increases in pH of the effluent during low-salinity waterflooding experiments, McGuire et al. (2005) proposed in-situ generation of surfactants as a low-salinity mechanism. The rise in pH was believed to be generated by low-salinity water reacting with minerals present in the formation, yielding hydroxides ($OH^-$). This was suggested

to cause pH to increase from the 7 to 8 range, to 9 or more. At these levels, it was suggested that low-salinity waterflooding acts similar to alkaline flood, which enhances oil recovery by reduction of oil-water interfacial tension (IFT), inducing wettability alteration towards more water-wet, and mobilization of oil by emulsification [3]. Emulsification was later observed at the crude oil/low-salinity water interface by Sohrabi et al. (2015) [19]. In addition, increased pH is also believed to amplify mobilization of fines [20].

Despite reports of low-salinity mechanisms appearing to act similar to alkaline flooding [3], the effect of pH increase during low-salinity waterflooding is disputed. Coreflooding experiments have failed to show a clear relationship between the effluent pH and recovery, and the effluent pH is seldom comparable to alkaline flooding values [21].

### Wettability Alteration

Wettability alteration towards more water-wet is the most commonly suggested low-salinity mechanism [1]. However, it is not clear what causes the wettability to change. Several theories have been suggested, most frequently mentioned are multicomponent ion exchange and electrical double-layer expansion.

The electrical double layer model is a description of the ion distribution around negatively charged clay surface (see Figure 2.8). The innermost layer, called the adsorbed layer, consists positive ions that are strongly bound to the clay surface. The outermost layer, called the diffuse layer, contains dispersed ions that are more weakly bound to the clay. The distance between the clay surface and the point were no net charge is felt is called the double layer thickness. It has been proposed that the double layer expands during low-salinity waterflooding due to decreasing salinity, which reduces the adhesive forces between the clay and polar components present in crude oil. [22]

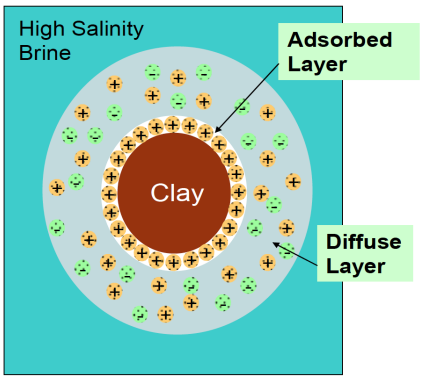


**Figure 2.8:** Schematic of the electrical double layer model. [22]

Lager et al. (2006) suggested multicomponent ionic exchange, commonly denoted MIE,

as a low-salinity mechanism causing wettability alteration. The mechanism may briefly be described as the detachment of polar organic compounds present in oil from the clay surface by cation exchange. Cation exchange substitutes organic polar compounds bound directly to the clay surface and organometallic complexes bound by ligand bonds to the clay surface, yielding wettability alteration towards more water-wet. [8]

### 2.1.4 Low-Salinity Mechanisms in Carbonates

Carbonate reservoirs are typically characterized as highly fractured reservoirs containing low-permeability mixed/oil-wet matrix blocks with high-porosity. Hence, carbonate reservoirs differ significantly from sandstone reservoirs, which tend to be mixed/water-wet. This difference is related to carbonates having a positively charged surface, while sandstones have a negatively charged surface. [11]

To produce oil from fractured reservoirs water must imbibe into the matrix blocks and displace oil into the fractures. Due to unfavorable wettability regimes, the spontaneous imbibition process ceases when there is still significant amounts of mobile oil left in the matrix blocks. Wettability is, therefore, crucial to the performance of carbonate reservoirs and factors affecting the wettability of carbonates is subject to extensive research. Two of these factors are the brine salinity and ionic composition. [11]

#### Influence of Ionic Composition

In contrast to the low-salinity mechanisms mentioned earlier for sandstones, there are several reports of increased oil recovery from carbonates by increasing the concentration of certain ions. Surface active anions such as sulfate ($SO_4^{2-}$) have been reported to cause wettability modification towards more water-wet in some carbonates [23, 24, 25]. There are also reports of borate ($BO_3^{3-}$) and phosphate ($PO_4^{3-}$) having similar effects [11]. Increasing the concentration of cations such as calcium ($Ca^{2+}$) and magnesium ($Mg^{2+}$) have also been reported to contribute to increased oil recovery in the presence of sulfate [24, 25, 26].

The effect of surface active ions has, among others, been observed in laboratory studies on Stevns Klint outcrop chalk, which is widely used as a North Sea chalk analog [27]. Strand et al. (2006) suggested that the underlying mechanism in chalk formations was wettability alteration due to adsorption of sulfate to the chalk surface and co-adsorption of calcium ions causing desorption of negatively charged organic compounds present in crude oil (see Figure 2.9) [24]. Strand et al. (2008) reported that brine containing $SO_4^{2-}$, $Ca^{2+}$ and $Mg^{2+}$ had an effect on the wettability of limestone; however, it is believed to have a smaller effect in limestone than chalk [28].

Due to the abundance of sulfate in seawater, brine composition is believed to be an important cause of the increased oil production observed in the Ekofisk field after initiation of seawater injection [11]. Note that injection of seawater is not considered to be low-salinity water injection.

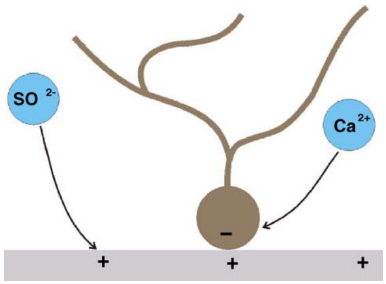


**Figure 2.9:** Schematic of mechanism causing wettability alteration in carbonates. [24]

### Influence of Brine Salinity

Other studies on carbonates report that lowering the water salinity caused wettability alteration towards more water-wet. Almehaideb et al. (2004) observed in contact angle measurements on limestone samples that there was a wettability alteration towards more water-wet when salinity changed from $0\ ppm$ to $10,000\ ppm$, and wettability alteration towards more oil-wet when salinity changed from $10,000\ ppm$ to $50,000\ ppm$. Based on this study it was concluded that there was an optimum salinity for carbonate wettability [29].

Alotaibi et al. (2010) also reported a clear trend that lowering the brine salinity resulted in wettability change towards more water-wet during contact-angle measurements on calcite crystal and limestone samples [30]. However, the brines used in this experiment did not only vary in salinity, they also varied in relative ionic composition, where the concentration of sulfate was higher in seawater and aquifer water than formation water, despite having lower salinity.

Yousef et al. (2010) reported significant incremental oil recovery from coreflooding experiments using composite carbonate cores a synthetic seawater solution as the injection fluid. Brine was injected until no more oil was being produced, followed by sequentially dilution of the initial brine, thus maintaining the relative ionic composition throughout the experiment. Results from one coreflooding experiment can be seen in Figure 2.10. Incremental recovery had the great effect when diluting the brine from $57,670\ ppm$ to $5,767\ ppm$, and little effect when diluting from $5,767\ ppm$ to $578\ ppm$. IFT measurements showed that the effect of dilution on fluid-fluid interactions was negligible. Incremental increases in oil recovery were therefore attributed to wettability alteration. [31]

Rumanuka et al. (2012) performed an extensive study of wettability alteration in carbonates. Wettability alteration was assessed using spontaneous imbibition tests on chalk, limestones, and dolomites. Both the brine salinities and concentrations of sulfate were varied. The results of the study (see Figure 2.11) showed a large scatter in incremental recoveries with the majority of high recoveries observed at low salinities and only a chalk sample showing higher recovery with higher sulfate concentrations.

As we can see, the effects of brine salinity on oil recovery in carbonates is complex as

brine salinity, ionic composition and the formation type influence the recovery.

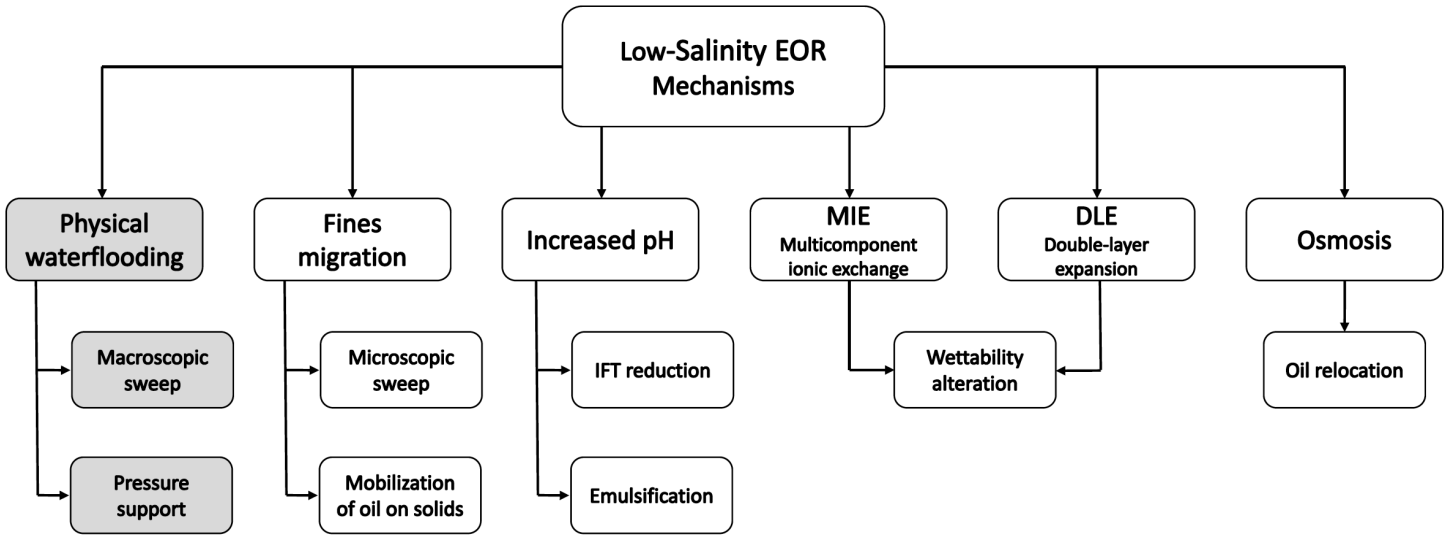


**Figure 2.7:** Overview of proposed low-salinity recovery mechanisms for sandstones and how they contribute to oil recovery. Macroscopic sweep and pressure support are also achieved by conventional waterflooding.

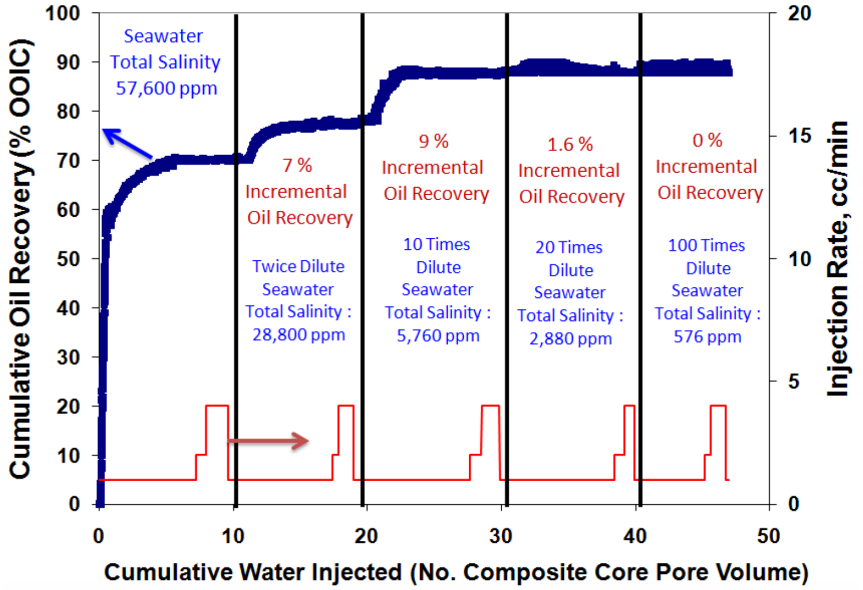


**Figure 2.10:** Oil recovery (blue) and water injection rates (red) vs. cumulative injected water. Coreflooding using composite carbonate cores. Sequential dilution of the initial brine results in significant incremental oil recovery when diluting from $57,670\ ppm$ to $5,767\ ppm$. [31]

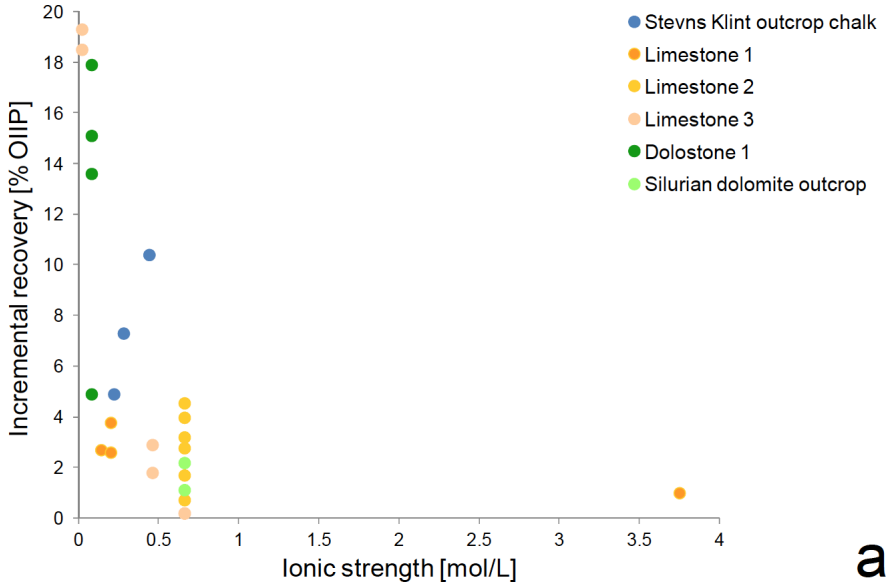


**(a)** Incremental recovery (increased oil recovery) vs. ionic strength (salinity).

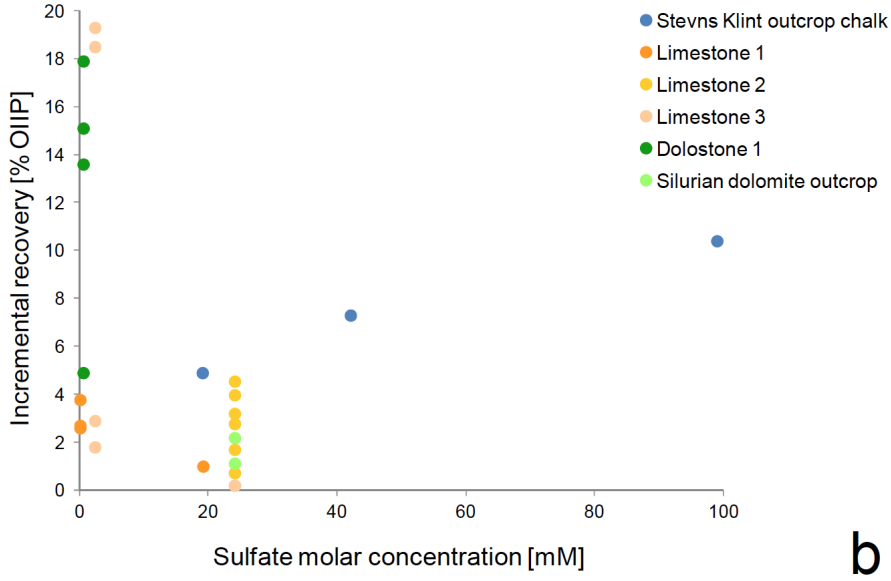


**(b)** Incremental recovery (increased oil recovery) vs. sulphate concentration

**Figure 2.11:** Results of spontaneous imbibition tests on carbonates using different salinities and brine compositions. [27]

## 2.2 Osmosis as a Mechanism for Low-Salinity EOR

Osmosis was proposed as a low-salinity mechanism by Sandengen and Arntzen (2013) who hypothesized that oil acts as a semi-permeable membrane that passes water but not ions. It was suggested that in a fluid system containing low-salinity water, high-salinity water and oil, where the water phases are physically separated by oil, pure water passes through the oil into the high-salinity water pockets. This causes the pockets of high-salinity water to expand, the low-salinity water to contract and a relocation of the surrounding oil. [32]

### 2.2.1 Visualization Experiments Using Capillary Tubes

Sandengen and Arntzen (2013) reported observations of oil droplets moving under the influence of an osmotic gradient. The experimental setup consisted of a glass capillary tube with high-salinity brine enclosed by two oil droplets and distilled water outside the oil (see Figure 2.12). After 12 days the oil droplets had clearly moved away from each other and the high-salinity water had expanded (see Figure 2.13). [32]

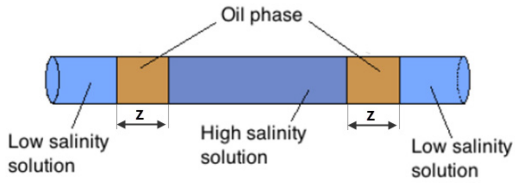


**Figure 2.12:** Schematic of setup of 1D visualization experiment performed by Sandengen and Arntzen (2013). [32]

Sandengen and Arntzen (2013) suggested that low-salinity waterflooding could contribute to increased oil recovery through microscopic water diversion, i.e. water being transported away from the main flow paths into the less conductive parts of the pore space by diffusion through oil membranes. Systems consisting of oil-wet formation at high temperature, with high oil saturation and a wide pore size distribution were suggested as most suitable to achieve a significant contribution from osmosis. [32]

The use of water-wet glass capillary tubes caused uncertainty of whether the transport mechanism was bulk diffusion of water through the oil phase, as predicted by osmosis, or diffusion along the water film on the tube edges. Fredriksen et al. (2017) performed a similar experiment on oil-wet polytetrafluoroethylene (PFTE) capillary tubes in order to restrict film flow along tubing walls. Both expansion of the high-salinity water contraction of the low-salinity water was observed and it was concluded that water was transported by bulk diffusion through the oil. [33]

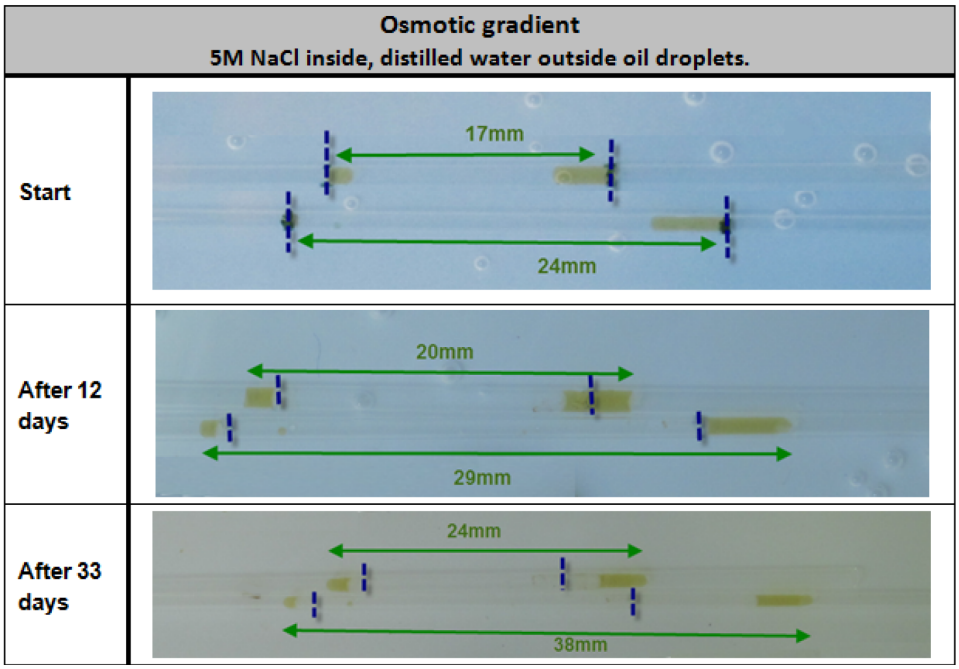


**Figure 2.13:** Results of 1D visualization experiment performed by Sandengen and Arntzen (2013). The results show oil droplets moving under the influence of an osmotic gradient. [32]

### 2.2.2 Visualization Experiments Using 2D Micromodels

Sandengen et al. (2016) extended the visualization experiment from 1D capillary tubes to 2D micromodels. For osmosis to have any effect during low-salinity waterflooding, complete separation of high-salinity water and low-salinity water by oil is required. In the first part of their experiments, Sandengen et al. (2016) investigated the presence of stable encapsulations of connate water at tertiary conditions, i.e. near residual oil saturation ($S_{or}$). High-salinity brine was used as connate water and toluene as the oil phase. Oil-wet and water-wet soda-glass micromodels were saturated with high-salinity brine, drained by toluene-flooding and flooded by high-salinity brine until residual oil saturation was reached. At this point, no osmotic gradient had been established. It was observed that brine was effectively trapped by the oil phase in the oil-wet micromodel (see Figure 2.14a) while the water-wet micromodel was unsuccessful in establishing stable pore-sized encapsulations of connate water by oil due to continuous water films on the grain surfaces (see Figure 2.14b). [34]

After stable encapsulations of connate water had been verified, low-salinity waterflooding was initiated in the oil-wet micromodel. Deionized water was used as the low-salinity water. An osmotic gradient was established and connate water expansion was observed. Connate water expansion continued until the encapsulating oil film ruptured. Figure 2.15

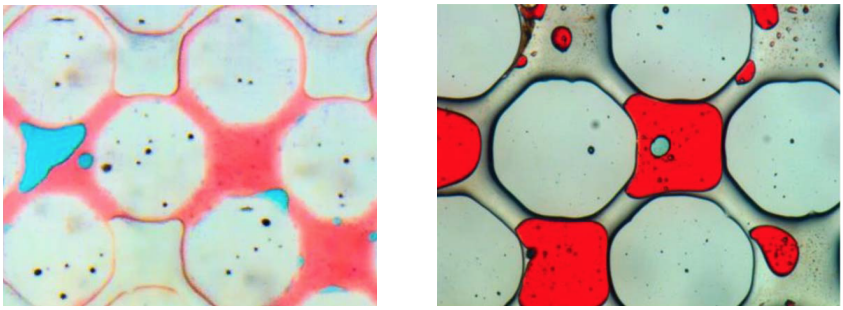

**(a)** Oil-wet micromodel **(b)** Water-wet micromodel

**Figure 2.14:** High-salinity brine (blue) was used as connate water, toluene (red) as oil phase, and high-salinity brine (uncolored) as injection fluid. Stable encapsulations of connate water were observed in the oil-wet micromodel, but not the water-wet micromodel. [34]

shows the complete waterflooding sequence initiated after the visual verification of the stable connate water encapsulations.

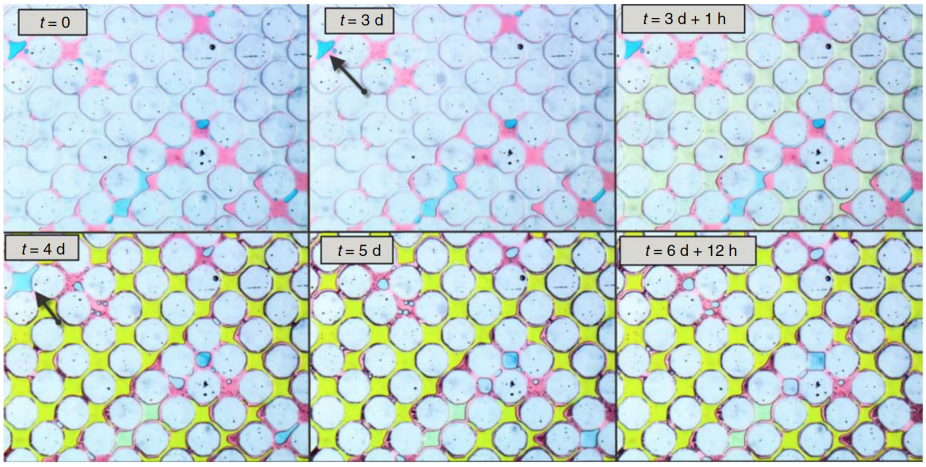


**Figure 2.15:** The time sequence shows connate water expansion during low-salinity waterflooding. High-salinity brine (blue) was used as connate water, toluene (red) as oil phase, high-salinity brine (uncolored) as initial injection fluid and deionized water (yellow) as injection fluid. Injection fluid was changed from high-salinity brine to deionized water after 3 days. The black arrows indicate an enclosed connate water pocket that expands until it ruptures after 4 days. Connate water expansion is also observed at the middle-right of the model. [34]

Connate water contraction was observed in a similar experiment performed when using deionized water as connate water and high-salinity brine as injection fluid. The inversion of the salinities implies an opposite osmotic gradient and the resulting connate water

contraction (see Figure 2.16) is in accordance with the hypothesis that pure water passes through oil from high-salinity water to low-salinity water.

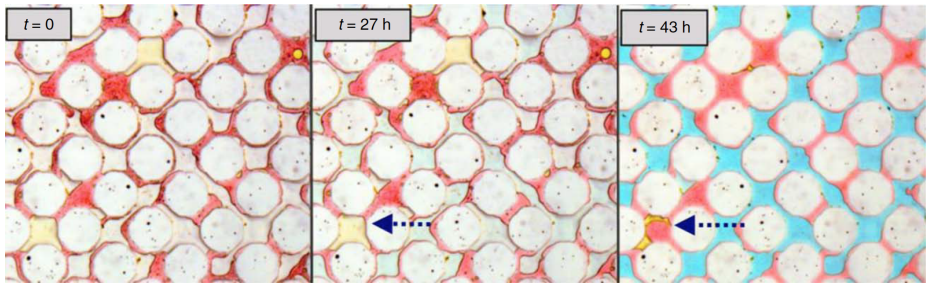


**Figure 2.16:** The time sequence shows connate water contraction during high-salinity waterflooding. Deionized water (yellow) was used as connate water, toluene (red) as oil phase, deionized water as initial injection fluid (uncolored) and high-salinity brine (blue) as injection fluid. Injection fluid is changed from deionized water to high-salinity brine after 27 hours. The blue arrow indicates connate water contraction. [34]

The experiments performed by Sandengen et al. (2016) on soda-glass micromodels show the ability of low-salinity waterflooding to induce connate water expansion and oil relocation by osmosis. Further, to investigate if osmosis could also increase oil production, a second experiment was performed using an oil-wet silicon-wafer micromodel with an adjacent flow channel used to mimic a fracture system. Residual oil saturation was established in the model using high-salinity brine and toluene. Low-salinity water was then flooded through the adjacent flow channel. Connate water expansion, displacement of oil towards the flow channel and oil dislodging from the matrix into the flow channel was observed (see Figure 2.17). Oil dislodging from the matrix into the flow channel is believed to be oil production by osmosis-induced microscopic water diversion.

Fredriksen et al. (2017) performed tests on similar silicon-wafer micromodels to investigate how wettability affects osmosis [33]. For oil-wet conditions, expansion of capillary trapped high-salinity brine and displacement of oil towards the flow channel was observed (see Figure 2.18), similar to the results reported by Sandengen et al. (2016). For strongly water-wet conditions, expansion of small dispersed droplets, present as water-in-oil microemulsion in the oil phase, was observed. Swelling of the oil phase caused displacement of oil towards the flow channel (see Figure 2.19).

Similarly to the observations of Fredriksen et al. (2017) under strongly water-wet condition, Sandengen et al. (2016) reported changes in the transparency of toluene when changing injection water in the soda-glass micromodel experiments.

### 2.2.3 Visualization Experiments Using Oil-Wet Sandstone Cores

Sandengen et al. (2016) also extended the visualization experiment to 3D using 5 $mm$ diameter sandstone cores [34]. Bentheimer sandstone core plugs were treated to obtain plugs with three different wetting regimes (water-wet, oil/mixed-wet, and oil-wet), two

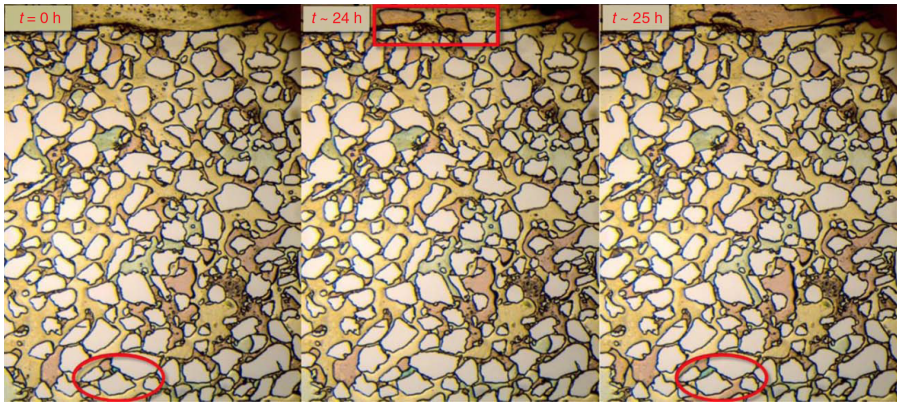


**Figure 2.17:** The time sequence shows connate water expansion during low-salinity flooding in the adjacent water channel at the top. High-salinity brine (blue) was used as connate water, toluene (red) as oil phase and deionized water (yellow) as low-salinity water. The red rectangle indicates oil being expelled from the matrix into the flow channel and the red rings indicate connate water expansion. [34]

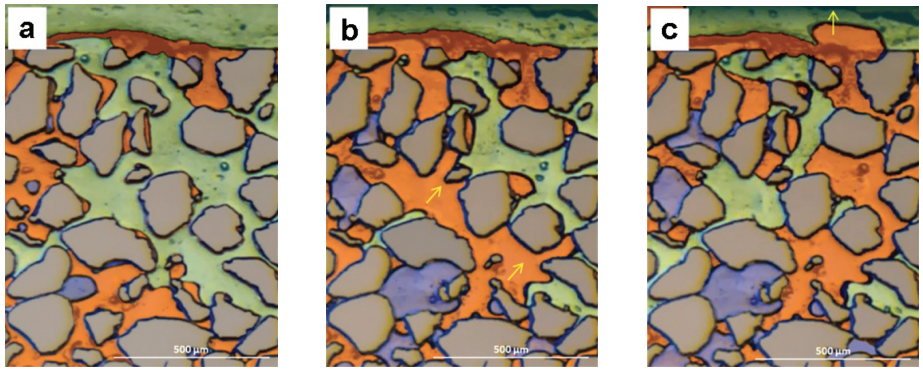


**(a)** Initiation of low-salinity waterflooding.

**(b)** Connate water expansion.

**(c)** Oil production.

**Figure 2.18:** The time sequence shows connate water expansion during low-salinity flooding in an oil-wet silicon-wafer micromodel. Low-salinity water in the adjacent water channel at the top. High-salinity brine (purple) was used as connate water, toluene (orange) as oil phase and deionized water (green) as low-salinity water. Yellow arrows indicate oil displaced towards flow channel caused by connate water expansion. [33]

plugs of each. The plugs were saturated with connate water ($5\frac{mol}{l}\ NaI$) and drained with oil (toluene). Subsequently, one core from each wetting regime was placed in high-salinity water ($5\frac{mol}{l}\ NaCl$) and one in low-salinity water (deionized water), and the cores were left to spontaneously imbibe.

Based on the theory of osmotic water transport it was expected that the enclosed pockets

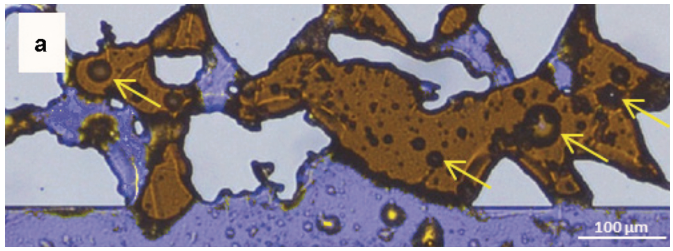


**(a)** Before low-salinity waterflooding.

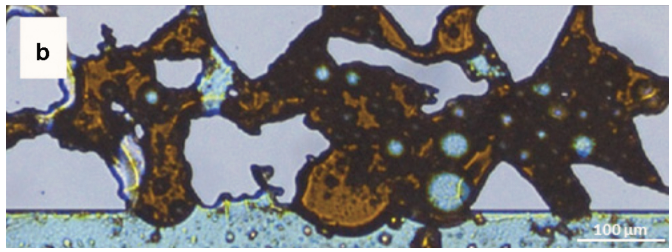


**(b)** Expansion of water-in-oil microemulsion.

**Figure 2.19:** The time sequence shows expansion of dispersed connate water droplets during low-salinity flooding in a strongly water-wet silicon-wafer micromodel. Low-salinity water is flooded along the flow channel at the bottom. High-salinity brine (purple) was used as connate water, crude oil (brown) as oil phase and deionized water (blue) as low-salinity water. Yellow arrows indicate dispersed droplets of brine in the oil. [33]

of connate water would be preserved in the high-salinity cases because there is no osmotic gradient. Enclosed pockets of connate water in cores submerged in low-salinity water, however, were expected to disappear due to connate water expansion causing the enclosing oil film to rupture. The results of the experiment are shown in Figure 2.20. Images of the cores showed that enclosed pockets of $NaI$ solution were more recurrent in the samples placed in high-salinity water than low-salinity water for all samples except the water-wet core plugs.

After the initial experiment, the oil/mixed-wet core plug that had spontaneously imbibed in high-salinity water was placed in low-salinity water and observed for $48$ hours (see Figure 2.21). Expansion of connate water was observed until the oil film ruptured and high-salinity connate water diffused out of the pore.

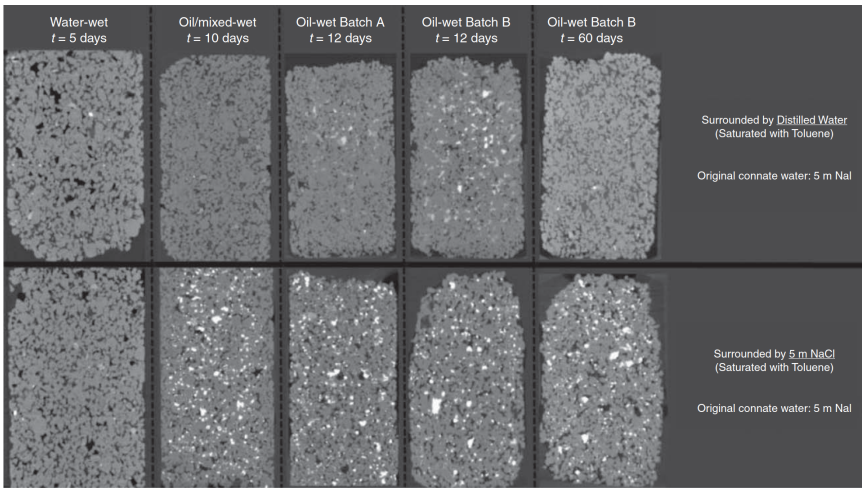


**Figure 2.20:** The micro-CT images show vertical cross sections of Bentheims sandstone cores with different wetting regimes after spontaneously imbibing in low-salinity water (top row) or high-salinity water (bottom row). $NaI$ solution, which was used as connate water, has high X-ray attenuation meaning that preserved pockets of $NaI$ will be visible as bright areas on the micro-CT images. [34]

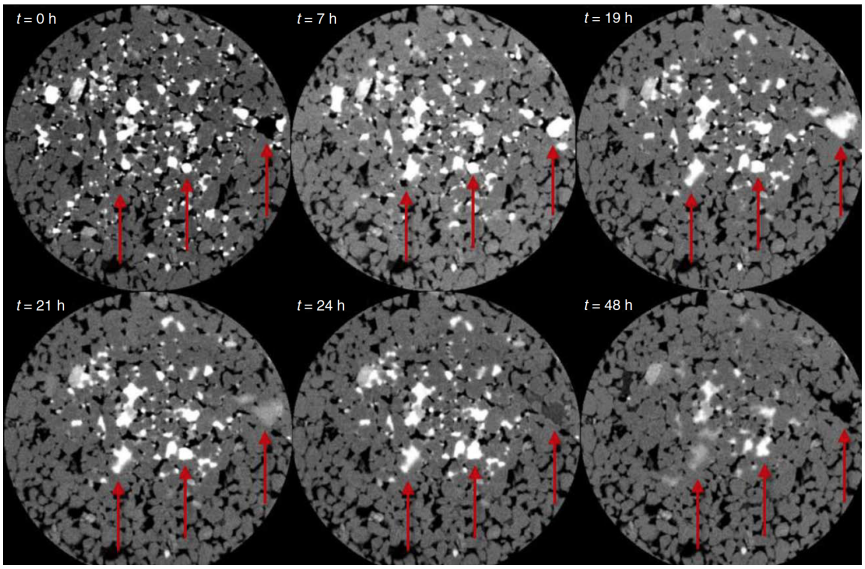


**Figure 2.21:** The time sequence of Micro-CT images shows connate water expansion during low-salinity imbibition in a mixed/oil-wet Bentheimer sandstone sample. Red arrows indicate connate water expansion. [34]

### 2.2.4 Current Research Results

The observations of water expansion or contraction seem to be in accordance with the theory on osmosis for all visualization experiments presented above. Hence, it is highly plausible that osmosis occurs during low-salinity waterflooding. It is also plausible that osmosis has the potential to act as a mechanism for low-salinity EOR. However, it is still uncertain whether the mechanism has any quantitative significance compared to other low-salinity effects. Bartels et al. (2010) reported from their micromodel experiments that osmosis was not a primary low-salinity mechanism [35].

To summarize the current status of research on osmosis as a mechanism for low-salinity EOR:

1. A hypothesis that osmosis can occur in a system containing low-salinity water, high-salinity water and oil has been proposed.
2. It has been reported that stable osmotic gradients may be established between enclosed pore-scale cavities of connate water and injection water under oil-wet conditions. This has been observed in one, two and three-dimensional visual experiments.
3. Both water expansion and contraction due to osmotic water transport through oil has been observed depending on the direction of the osmotic gradient. The behavior is in accordance with that suggested by osmosis theory.
4. Osmotic water transport has been observed in both oil-wet and strongly water-wet conditions. For oil-wet conditions, water transport occurs between the injected water and pore-scale cavities of connate water. For water-wet conditions, water transport occurs between the injected water and water droplets dispersed in the oil phase.
5. Osmotic water transport has been observed to cause relocation of oil. Favorable osmotic relocation of oil may mobilize the oil leading to increased oil recovery. This represents the EOR potential of osmosis as a low-salinity mechanism.

## 2.3 Osmotic Oil Relocation in Porous Media

Osmosis has been observed to cause simultaneous water expansion of high-salinity water and contraction of low-salinity water, resulting in relocation of oil. This effect may be described as an osmotic relocation of oil in the porous media. In a reservoir, osmotic oil relocation not believed to contribute directly to increased oil recovery. However, osmosis may contribute indirectly if oil relocation acts to mobilize initially immobile oil. One example of such favorable relocation is micro water diversion relocating bypassed oil into flow channels. [32, 34, 33]

Based on the mass balance principle, the net movement of oil, caused by osmotic relocation, across an arbitrary internal control volume in a homogeneous porous media is expected to be zero. This is because the amount of oil exiting the control volume is expected to be balanced by oil entering (see Figure 2.22).

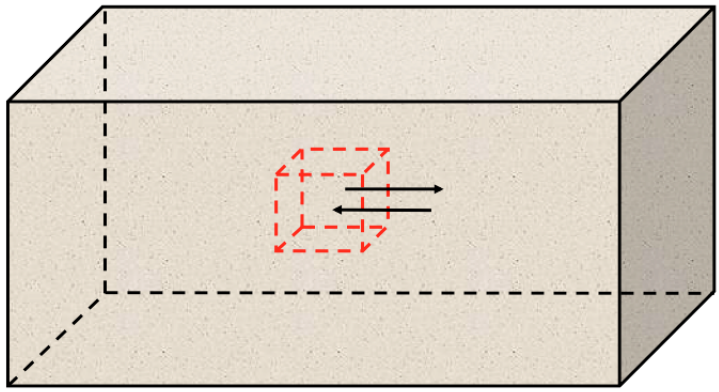

**Figure 2.22:** Schematic of control volume placed at an internal point in a homogeneous porous media body. The arrows illustrate that the amount of oil exiting the control volume is balanced by the amount of oil entering. This results in zero net movement out of the control volume.

However, if control surface completely or partially coincides with exposed surfaces, i.e. formation on one side and non-formation on the other, the amount of oil expelled from the control volume will not be balanced out by the oil entering and there will be a net movement of oil out of the control volume (see Figure 2.23). One examples of exposed surfaces are core surfaces in spontaneous imbibition tests or matrix block surfaces in fractured reservoirs. Based on mass balance, osmotic oil relocation will in such cases cause oil production proportional to the exposed surface area.

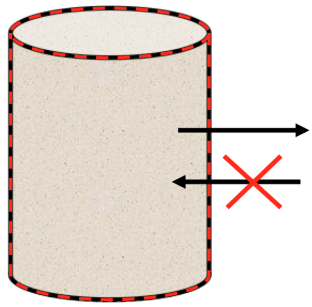

**Figure 2.23:** Schematic of control volume placed to coincide with exposed surfaces in a cylindrical porous media body. The arrows illustrate that the amount of oil exiting the control volume is not balanced by the amount of oil entering. This results in an expected net movement of oil out of the control volume.

In an effort to quantify the effect of osmosis during spontaneous imbibition in low-salinity water the following assumptions are made:

1. Osmosis causes random relocation of oil in homogeneous porous media. Hence, the effect of osmosis is sensitive to the surface area of porous media, but not volume.
2. The effect of other low-salinity EOR mechanisms are not sensitive to the surface area of the porous media.

Based on current knowledge of low-salinity mechanisms, osmosis seems to be the only proposed low-salinity mechanism where increased oil production correlates to surface area. However, the major uncertainty here is whether osmosis is the only mechanism sensitive to surface area. This is due to little attention being given to surface effects previously and the possibility of surface effects from undiscovered mechanisms.

If the assumptions are correct, the effect of osmotic oil relocation on increased oil production in spontaneous imbibition tests may be quantified by studying the relationship between surface area of the core and increased oil production. The relationship is expected to be linear yielding a curve that either intersects the y-axis at zero or a positive value depending on the contribution of other low-salinity mechanisms. An intersection at zero would indicate that only surface sensitive mechanisms, assumed to be osmosis, are active. An intersection at a positive value indicates a contribution from one or more low-salinity mechanisms that are sensitive to volume rather than surface area.

How to quantify the contribution of osmosis is illustrated in Figure 2.24 and is given by the following equation:

$$\Delta V_{LS,\,oil} = A \cdot \Delta v_{surface} + V_{pore} \cdot \Delta v_{volume} \tag{2.1}$$

$$\xrightarrow{assum.} \Delta V_{LS,\,oil} = A \cdot \Delta v_{osmosis} + V_{pore} \cdot \Delta v_{volume} \tag{2.2}$$

where

$\Delta V_{LS,\,oil}$ = Increased production by low-salinity water $[ml]$

$\Delta v_{surface}$ = Increased production per surface area due to surface effects $[\frac{cm^3}{cm^2}]$

$\Delta v_{osmosis}$ = Increased production per surface area due to osmotic relocation $[\frac{cm^3}{cm^2}]$

$\Delta v_{volume}$ = Increased production per surface area due to volume effects $[cm^3]$

$A$ = Surface area $[cm^2]$

$V_{pore}$ = Pore volume $[cm^3]$

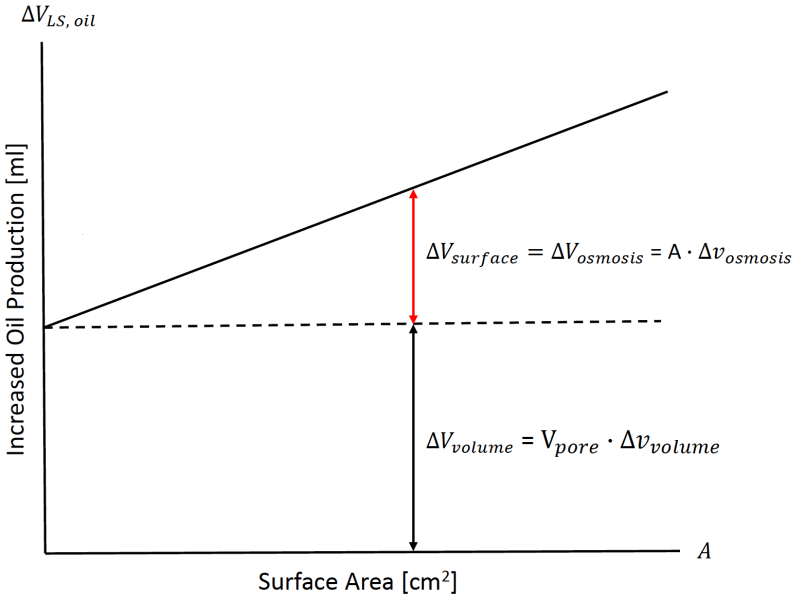


**Figure 2.24:** Illustration of surface area vs. increased oil production during low-salinity EOR. Based on the assumptions presented, a linear relationship is expected and the additional recovery from osmotic relocation may be quantified as $\Delta V_{osmosis}$.

Investigation of the relationship between $\Delta V_{LS,oil}$ and $A$ equivalent to be equivalent to investigating the relationship between recovery factor, approximated by $\frac{\Delta V_{LS,oil}}{V_{pore}}$, and the surface to volume ratio, $\frac{A}{V_{pore}}$.

Chapter 3

# Theory

## 3.1 Molecular Diffusion

Molecular diffusion is the net movement of molecules within a stagnant single phase that results from concentration gradients. Molecular diffusion can be described mathematically by Fick's first and second law. [36]

Fick's first law describes diffusion under steady-state conditions and states that the diffusion rate is proportional to the spatial concentration gradient. The steady-state diffusion flux vector is determined by:

$$\mathbf{J} = -D \, \nabla c \tag{3.1}$$

where

$\mathbf{J}$ = diffusion flux vector $\quad [\frac{mol}{m^2 \cdot s}]$

$D$ = diffusion coefficient $\quad [\frac{m^2}{s}]$

$c$ = concentration $\quad [\frac{mol}{m^3}]$

From Eq. (3.1) it is apparent that diffusion causes movement from high concentration areas to low concentration areas.

Fick's second law describes how diffusion changes with time. It is a partial differential equation that can be derived by applying Fick's first law, Eq. (3.1), and mass balance on a small control volume. The general form of Fick's second law is:

$$\frac{\partial c}{\partial t} = D \, \nabla^2 c \tag{3.2}$$

### 3.1.1 The Diffusion Coefficient

The diffusion coefficients used in Eq. (3.1) and Eq. (3.2) describe how well a stagnant fluid transports molecules along a given path. Important parameters affecting the diffusion coefficient are, therefore, the characteristics of the diffusion path. Intuitively, diffusion along straight paths is more efficient than diffusion along tortuous paths with constrictions.

The bulk diffusion coefficient ($D_0$) describes diffusion along a straight path with constant drift velocity. The coefficient is a measure the stagnant fluid's ability to transport molecules and can be approximated by Stokes-Einstein equations, which was originally derived for spherical particles diffusing at low Reynolds number [36]:

$$D_0 = \frac{k_B T}{6\pi\mu r} \tag{3.3}$$

where

$$\begin{aligned} k_B &= \text{Boltzmann's constant} && [\frac{J}{K}] \\ T &= \text{temperature} && [K] \\ \mu &= \text{viscosity} && [Pa \cdot s] \\ r &= \text{droplet radius} && [m] \end{aligned}$$

To describe diffusion in the case along tortuous paths with constrictions it is necessary to determine the effective diffusion coefficient ($D_e$). If both the bulk diffusion coefficient and the geometry of the flow path are known, the effective diffusion coefficient may be determined by [37]:

$$D_e = D_0 \frac{\tau^2}{C} \tag{3.4}$$

where

$$\begin{aligned} \tau &= \text{tortuosity} && [-] \\ C &= \text{constriction factor} && [-] \end{aligned}$$

Tortuosity is used to correct for deviations from shortest path and is defined as [38]:

$$\tau = \frac{l}{s} \tag{3.5}$$

where

$$\begin{aligned} s &= \text{straight-line length} && [m] \\ l &= \text{flow path length} && [m] \end{aligned}$$

The constriction factor is used correct for deviations in drift velocity caused by variations in cross-sectional area and may be determined by [38]:

$$C = \frac{1}{l^2} \int_0^l A(x)dx \int_0^l \frac{1}{A(x)}dx \tag{3.6}$$

where

$$x = \text{position along flow path} \qquad [m]$$
$$A(x) = \text{cross-sectional area at x} \qquad [m^2]$$

For a straight tube with constant cross-section the tortuosity factor $\tau = 1$ and the constriction factor $C = 1$. Hence, by Eq. 3.4 the effective diffusion coefficient is equal to the bulk diffusion coefficient, i.e. $D_e = D_0$.

### 3.1.2 Solution to One-Dimensional Diffusion Equation

Using Fourier series and the method of separating variables, it is possible to derive an analytical one-dimensional solution to Eq. 3.2 [39]. Applying initial conditions $c(x, t = 0) = c_0$ and boundary conditions $c(x = 0, t) = c(x = L, t) = 0$ the following solution may be derived:

$$c(x,t) = \sum_{n=1}^{\infty} \frac{2}{n\pi} c_0 \big(1 - (-1)^n\big) sin(\frac{n\pi x}{L}) e^{-\frac{L^2}{n^2\pi^2 D_e}t} \tag{3.7}$$

where $c(x, t)$ represents the salinity at given position ($x$) and time ($t$) in a one-dimensional porous media of length $L$.

For spontaneous imbibition tests using distilled water as the imbibing phase, the solution presented in Eq. 3.7 can be used to estimate the time needed for dissolved salts to diffuse out of the core through the continuous water films. By choosing length $L$ equal the thickness of the core ($z$), the solution may be used to obtain an estimate of the salt concentration in the core at a given time. Note that in an actual spontaneous imbibition test diffusion will occur in multiple directions. The actual diffusion process will, therefore, be more efficient than the one-dimensional estimate (see Figure 3.1).

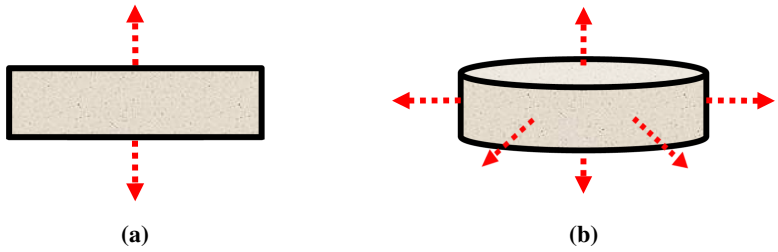


**Figure 3.1:** Comparison of (a) 1D diffusion and (b) 3D diffusion.

## 3.2 Diffusion Processes During Low-Salinity Waterflooding

During low-salinity waterflooding, there are two relevant diffusion processes happening. These are diffusion of dissolved salt along continuous water paths and diffusion of water droplets through oil membranes.

### 3.2.1 Salt Diffusion

Diffusion of dissolved salt will occur along continuous water paths due to concentration differences. When a core saturated with high-salinity water and oil is submerged in low-salinity water, such as in a low-salinity spontaneous imbibition test, the concentration difference will cause dissolved salts in the core to diffuse along continuous water paths out of the core. The diffusion process will continue until there is no longer a concentration gradient, i.e. when the salinity inside and outside the core are equal.

The diffusion process described here does not affect dissolved salts that are disconnected from the continuous water paths connected to the low-salinity water. Hence, it is possible to obtain pockets of high-salinity water enclosed by oil, that are surrounded by low-salinity water. Several examples of configurations like this were presented in Section 2.2 and are required for osmosis to occur.

### 3.2.2 Water-in-Oil Diffusion

As mentioned in Section 2.2, in a fluid system consisting of low-salinity and high-salinity water completely separated by oil, it has been hypothesized that oil will act as a semipermeable membrane allowing water to pass but not ions [32].

Although oil and water solutions are commonly treated as immiscible fluids, small quantities of water can dissolve in oil. Likewise, small quantities of oil can dissolve in water. The mutual solubilities of water and oil depend on the salinity of the water. In general, the solubility of water in oil at equilibrium with low-salinity water is larger than the solubility of water in oil at equilibrium with high-salinity water [32].

In an oil that is in equilibrium with high-salinity water on one side and low-salinity water on the other, there will be a concentration gradient of dissolved water. As a consequence, dissolved water will diffuse from the low-salinity to high-salinity water through the oil phase.

Applying Fick's first law (Eq. 3.1), the diffusion rate of water through oil can be determined by,

$$\mathbf{J} = -D \, \nabla c_w \tag{3.8}$$

where $c_w$ is water-in-oil solubility. Note that it is the gradient of dissolved water that determines the diffusion rate, not the salinity gradient.

The rate of one-dimensional osmotic water transport may be approximated by:

$$J = D\frac{\Delta c_w}{z} \tag{3.9}$$

where $z$ is the thickness of the oil membrane. The concentration of water in oil at the oil/brine interface may be expressed by [34]:

$$c_{brine} = c_0 \; a_{brine} \tag{3.10}$$

where $a_{brine}$ is the activity of water in brine and $c_0$ is the water-in-oil solubility for oil in equilibrium with pure water. The rate of osmotic water transport through an oil membrane separating pure water and brine can then be approximated using:

$$J = D \; c_0 \; \frac{(1 - a_{brine})}{z} \tag{3.11}$$

Chapter 4

# Methods

## 4.1 Experimental Design

Increased oil recovery due to osmosis is expected to have a stronger correlation to the surface-to-volume ratio than other low-salinity EOR mechanisms. As argued in Section 2.3, it is expected that the increased oil recovery from osmotic oil relocation will be proportional to the area of exposed surfaces. In addition, it is believed that choosing cores and fluids with certain properties can further isolate the osmosis as the main low-salinity mechanism during experiments.

The experiment proposed is a low-salinity spontaneous imbibition experiment using core samples with different surface-to-volume ratios. Selection of the core and fluids are made in order to facilitate increased oil recovery by osmosis-induced connate water expansion. Considerations have also been made to reduce the contributions other proposed low-salinity mechanisms. Fluid selection has also made to achieve osmotic water transport rates comparable to what is expected at reservoir temperature.

### 4.1.1 Core Selection

As mentioned in section 2.2.2, osmotic water transport has been reported under both water-wet and oil-wet conditions. However, it is believed that oil-wet conditions are more ideal for osmosis [34, 33]. This is because the expansion of enclosed connate water pockets, which are not stable under water-wet conditions, is believed to have larger effect on oil recovery than the expansion of dispersed water droplets in oil.

Based on the available literature it seems that low-salinity water effects on carbonates are less understood compared to sandstones. Although osmosis as a low-salinity EOR mechanisms is, at least in theory, independent of the rock type, our lack of knowledge impairs our

ability to isolate the osmotic effect from the contribution of other mechanisms in carbonates. Therefore it seems most appropriate to analyze osmosis in sandstone samples.

Consequently, it is desirable to use oil-wet sandstone cores. Reservoir sandstones are seldom expected to be strongly oil-wet. To obtain an oil-wet sandstone it is possible to treat the cores by silane surface modification [40, 34]. Therefore, it was decided to use samples of Bentheimer sandstone that had been treated to obtain oil-wet regime.

The procedure used to render the cores oil-wet is as follows: The cores were treated with hexamethyldisilazane (HMDS) at $90^oC$, rinsed with hexane at $60^oC$ and dried at $80^oC$.

Bentheimer sandstone was chosen because it has low clay content, typically below $5\%$ [41], which can reduce effects of clay destabilization. The silane surface treatment is also believed to mitigate both the effects of clay destabilization and the effects of wettability alteration. This will be discussed further in Section 6.2.

### 4.1.2 Fluid Selection

The process of selecting fluids for the experiment was mainly focused on achieving a water-in-oil diffusion rate comparable to those in field cases.

Large differences in salinity will cause both rapid diffusion of dissolved salts out of the core and diffusion of water through oil. From Eq. 3.11 we can see that the diffusion rate of water through oil improves by increasing the water-in-oil solubility [34]. Water is generally more soluble in alkylbenzenes than normal alkanes [42]. In addition, the solubility of water in hydrocarbons typically increase with increasing temperature [42] and decrease with increasing salinity [32].

Isolating the effect of osmosis was also taken into consideration in fluid selection. Studies have reported that crude oil with polar compounds is necessary to achieve any significant increased oil recovery by low-salinity waterflooding [17, 21]. As discussed in Section 2.1.3, wettability alteration theories typically describe the alteration as a result of changes in the electrostatic bonds between grain surfaces and organic polar components typically found in crude oils. Using a refined oil without polar components can, therefore, be used for mitigating the effect of wettability alteration.

Based on these considerations, it is reasonable to choose water phases with large differences in salinity and a refined oil with high water-in-oil solubility. It was decided to use $5\frac{mol}{l}$ sodium chloride ($NaCl$) solution as high-salinity water, distilled water as low-salinity water and toluene (methylbenzene, $C_7H_8$), an alkylbenzene, as the oil phase. Toluene was colored red for visibility purposes by adding Oil Red O. Sandengen et al. (2013) estimated that these fluids will at ambient conditions yield a diffusion rate comparable to that in North Sea reservoir oils at $80 - 100^oC$ [32].

Using Eq. 3.7 it is possible to estimate the time for dissolved salt to diffuse out of the core. Berg (2012) estimated tortuosity and constriction factors for Bentheimer core plugs to be $\tau = 0.612$ and $C = 1.924$ [38]. The bulk diffusion coefficient for $5\frac{mol}{l}$ $NaCl$ at $25^oC$

has been measured to be $D_0 = 5.168 \cdot 10^{-9} \frac{m^2}{s}$ [43]. The length of the porous media ($L$) is set equal to the height of the largest core height, $z = 0.025\ m$ (sample A). By including the first $500$ terms of the solution it was observed that most of the salt had diffused out within 3 days (see Figure 4.1). For the smallest core slices (sample D) most of the salt had diffused out within 3 hours

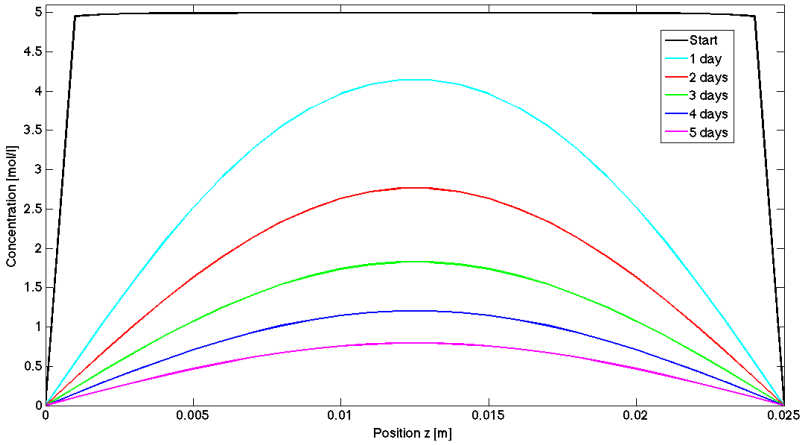


**Figure 4.1:** Salt concentration vs. at position x over time. Initially, the salinity is $c_0 = 5.0 \frac{mol}{l}$ throughout the core and zero outside the core. Core boundaries at $z = 0.0$ and $z = L = 3.8 \cdot 10^{-3}\ m$. MATLAB was used for calculations and plots.

Alkylbenzenes are more soluble in water than normal alkanes [42]. To avoid produced oil being dissolved in water, the water solutions used in the Amott cells had to be equilibrated with toluene ahead of the experiment. The solubility of alkylbenzenes in water has a minimum at $\approx 291K$ and increases with increasing temperature. Therefore, the water solutions should ideally be equilibrated with toluene at the same temperature being used for the imbibition experiment.

## 4.2 Experimental Procedure

A workflow summary of the experimental procedure followed is given in Figure 4.2. The experiment was performed twice using the same core samples. The first experiment was performed at elevated temperature ($70^oC$) and the second at ambient temperature ($\approx 22^oC$). Work processes and storage were performed in fume hoods or ventilated ovens due to the volatility of toluene.

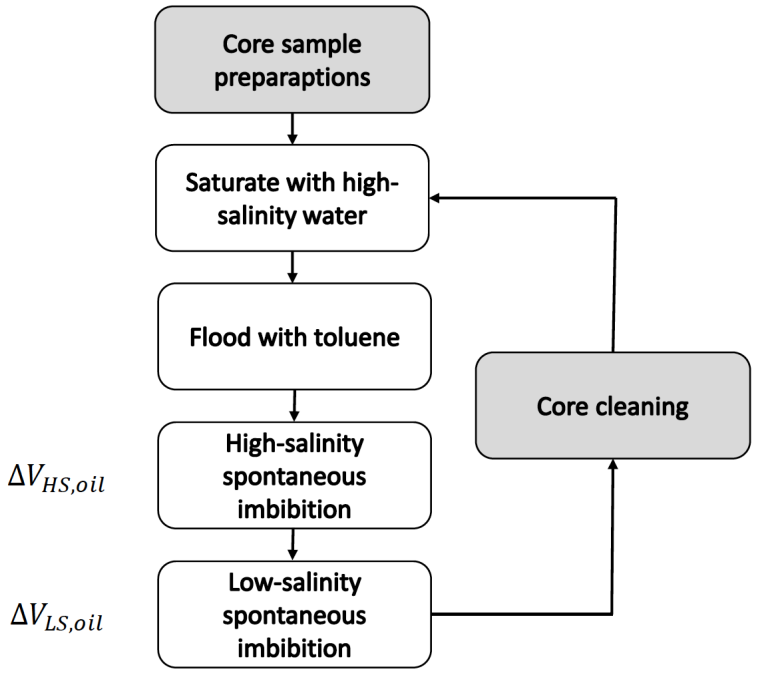


**Figure 4.2:** Work flow for experiment.

### 4.2.1 Core Preparations

#### Cutting

In order to obtain core samples with varying surface-volume ratios, two oil-wet Bentheimer core plugs were cut into smaller slices of various sizes. The cores were cut with a precision circular saw into ten slices, which constitutes four samples. Distilled water was used as a cooling agent during cutting. After cutting the cores were rinsed with distilled water to remove dust and left to dry at $40^oC$.

The core samples consisted of varying number of slices with approximate equal thickness. The number and size of slices per sample are given in Table 4.1.

**Table 4.1:** Table of core sample thicknesses and number of slices. All slices have the same radius.

| Sample | No. of Slices | Slice Thickness [mm] |
|---|---|---|
| A | 1 | 25 |
| B | 2 | 10 |
| C | 3 | 13 |
| D | 4 | 5 |

### Calculating Sample Bulk Volumes and Surface Areas

Thickness and diameter of each individual core slice were measured to account for small deviations during cutting and to improve the accuracy of volume and area calculations. A digital caliper was used to measure the cores. Bulk volumes and surface areas were calculated using averages of three measurements. The cores were rotated between each measurement to mitigate the effects of local discrepancies and the caliper was calibrated between measuring each slice.

The bulk volume ($V_{bulk}$) of each sample was calculated by:

$$V_{bulk} = \sum_{j=1}^{n} \frac{\pi}{4} d_j^2 \cdot z_j \tag{4.1}$$

where

$$\begin{aligned} n &= \text{number of core slices} && [-] \\ j &= \text{core slice number} && [-] \\ d_j &= \text{diameter of piece j} && [m] \\ z_j &= \text{thickness of piece j} && [m] \end{aligned}$$

The surface area ($A$) of each sample was calculated by:

$$A = \sum_{j=1}^{n} (\frac{\pi}{2} d_j^2 + \pi d_j z_j) \tag{4.2}$$

### Measuring Sample Pore Volumes and Porosities

Helium porosity was used to determine the pore volume of the samples. Porosity measurements were performed on core samples, i.e. several slices at once for samples B ,C and D. The resulting porosity, therefore, represents an average porosity for all slices in

the sample. Note that the helium porosity method measures effective porosity, excluding disconnected pores, and is not relevant for this experiment.

A helium porosity measurement consists of two volume measurements, the volume of gas in an empty chamber ($V_1$) and the volume of gas in a chamber containing a core sample ($V_2$). The helium porosity apparatus is shown in Figure 4.3. The difference between these measurements equals the sample grain volume ($V_{grain}$):

$$V_{grain} = V_1 - V_2 \tag{4.3}$$

where

$$\begin{aligned} V_{grain} &= \text{sample grain volume} && [m^3] \\ V_1 &= \text{volume of empty chamber} && [m^3] \\ V_2 &= \text{volume of chamber containing sample} && [m^3] \end{aligned}$$

Grain volumes were also calculated using the average of three $V_1$ and $V_2$ measurements.

The sample pore volumes ($V_{pore}$) were calculated by:

$$V_{pore} = V_{bulk} - V_{grain} \tag{4.4}$$

where

$$V_{pore} = \text{sample pore volume} \qquad [m^3]$$

From this, the effective porosities ($\phi_e$) were calculated by:

$$\phi_e = \frac{V_{pore}}{V_{bulk}} \tag{4.5}$$

where

$$\phi_e = \text{effective porosity} \qquad [-]$$


**Figure 4.3:** Helium porosity apparatus. Core chamber in front of large volume gauge.

### 4.2.2 Saturating Samples

To achieve initial saturation condition, i.e. high-salinity water and toluene at irreducible water saturation ($S_{wir}$), the core samples were first completely saturated with high-salinity water and subsequently drained by toluene-flooding.

#### Water Saturation

To ensure efficient water saturation, the samples were saturated with high-salinity water by using a vacuum pump. Reducing the pressure of the air in the pores prior to introduces the cores to water will cause the water to imbibe into the pore space due to the pressure difference. The vacuum pump apparatus is shown in figure 4.4.

The dry core samples were placed in an empty beaker inside the vacuum chamber, the chamber was sealed, the vacuum pump was turned on and the pressure inside the chamber was reduced to approximately $0.1$ bar. The beaker containing the cores was then filled with high-salinity water until the cores had been completely submerged in water. The vacuum pump was turned off and the cores left to imbibe in water in the vacuum chamber for $30$ minutes. The beaker was removed from the vacuum chamber and the core samples were kept submerged in water until right before initiation of toluene flooding.

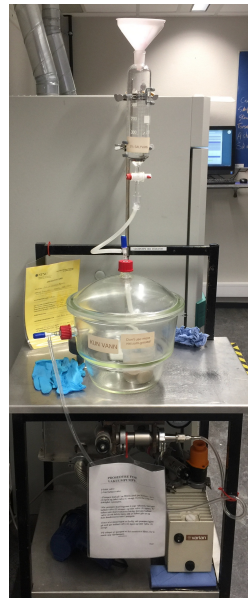

**Figure 4.4:** Vacuum pump apparatus for water saturation. From top to bottom: Water flask, vacuum chamber and compressor.

### Oil Saturation

After saturating the cores with high-salinity water, the cores were drained by toluene until irreducible water saturation, $S_{wir}$. The core-flooding apparatus consisted of a piston pump displacing Exxsol D60 into a fluid reservoir in which Exxsol D60 and toluene are separated by a sealing plug. During pumping Exxsol D60 is pumped into the fluid reservoir, pushing the plug and thus displacing the toluene out of the reservoir and through the core holder. The core holder consists of an inlet and outlet, and sleeve to apply confining pressure to the core by pressurized gas. The discharged fluid was collected in a beaker. The core-flooding setup is shown in Figure 4.5.

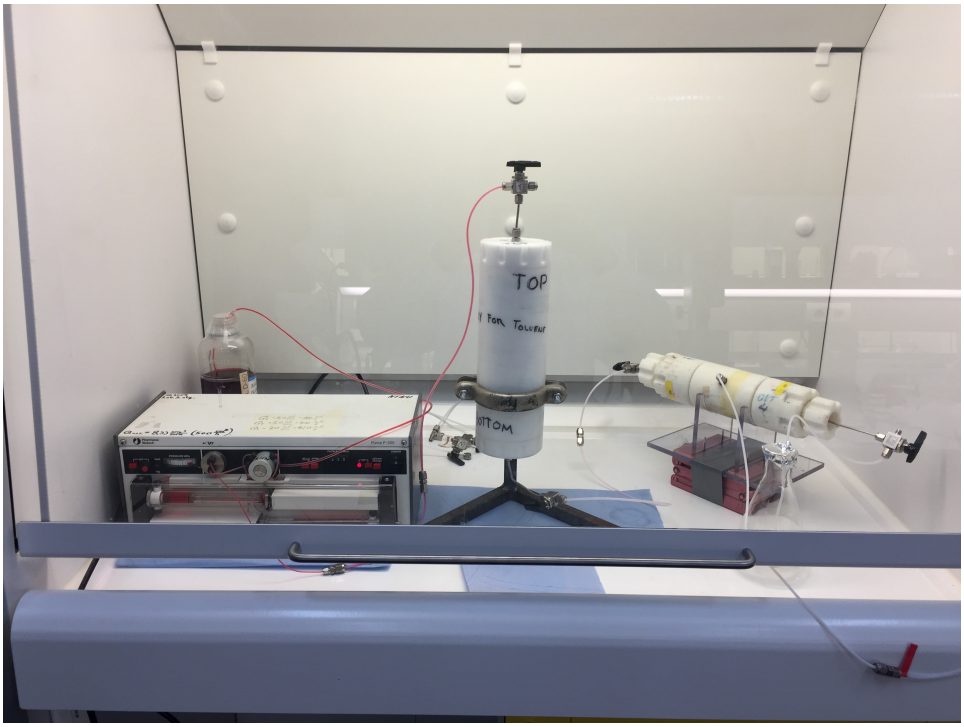


**Figure 4.5:** Toluene-flooding apparatus. From left to right: Piston pump, fluid reservoir, core holder and discharge beaker.

The core slices were assembled into one piece and placed inside the core holder (see Figure 4.6). The core slices were ordered from the smallest slices where placed near the inlet and the largest slices near the outlet. To maintain capillary continuity during flooding, and thus avoid end effects, filter papers were placed between the slices. Filter papers were also placed between the end cores and inlet and outlet. The filter papers were soaked in high-salinity water to improve cohesion between the core slices, simplifying the assembly of the cores.

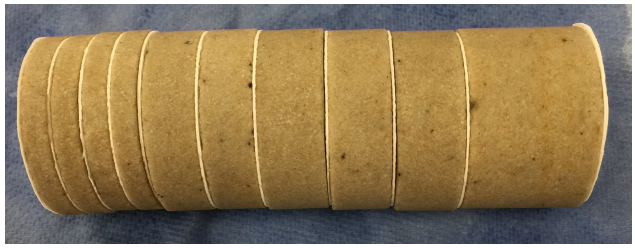

**Figure 4.6:** Assembled core consisting of all samples with filter paper between each core piece. The picture is taken prior to toluene-flooding core after the cores had been saturated with high-saline water. The left side was inserted near the inlet.

The core assembly was inserted into the core holder and secured tightly by adjusting the inlet and outlet plugs. A confining pressure of 11 bar was applied.

High flow rates followed by a bump rate was used to ensure proper drain the core. The flow rate was set to $7.0\frac{ml}{min}$ for at least 3 pore volumes (PV) followed by $8.33\frac{ml}{min}$ for at least 2 PV. To ensure that no more water was being produced, discharged liquids from the last couple of minutes of flooding was collected in a separate beaker and visually inspected for water before terminating the toluene-flooding.

After toluene-flooding was completed the cores were immediately removed from the core holder and submerged in toluene to prevent toluene evaporating and escaping from the pore space.

### 4.2.3 Spontaneous Imbibition in High-Salinity Water

Because of the relatively high solubility of toluene in water, a small amount of toluene was added to the high-salinity water to prevent dissolution of produced oil affecting the measurements. The beaker of brine and toluene was mixed together by shaking and stirring for approximately 30 minutes. The beaker was then left until all non-dissolved toluene had accumulated in a film on top of the water and removed using a syringe and paper towels.

Amott cells were filled nearly full with high-salinity water. One Amott cell was used per sample. The core slices were one by one removed from the toluene, shaken firmly 10-15 times to remove excessive toluene stuck to the core and placed in the Amott cell. To ensure maximum surface exposure of the core slices to water, pieces of plastic were placed in between the slices as spacers. High-salinity water was added until the cell was completely filled and the Amott cell was sealed. To ensure proper sealing of the cells the gaskets on the covers were properly cleaned and greased upon and the bolts tightened firmly using hand force.

For the experiment at elevated temperature, the Amott cells were stored in an oven at $70^oC$. To reduce thermal effects caused by the temperature dependency of oil solubility in water, high-salinity water used in this experiment was heated before being equilibrated with toluene and again before being added to the Amott cells.

The Amott cells were then left to spontaneously imbibe at given temperatures until oil production ceased. The amount of oil that had been produced was monitored daily when the oil production started to decrease. The cumulative produced oil volumes of each sample in high-salinity water ($\Delta V_{HS,i}$ where $i = A, B, C, D$) were recorded.

### 4.2.4 Spontaneous Imbibition in Low-Salinity Water

After all the spontaneous imbibition test had stabilized and oil production recorded, the Amott cells were opened and the content emptied into beakers. The cores were kept submerged in high-salinity. The Amott cell and plastics pieces were cleaned thoroughly us-

ing toluene and water, and rapidly dried using pressurized air and by being placed in an oven. When the Amott cells had dried, the cells were removed from the oven and left to cool.

The Amott cells were filled nearly full with low-salinity water, The low-salinity water had been toluene-saturated using the same procedure as described for high-salinity water. The core slices were one by one removed from the high-salinity water, shaken firmly 10-15 times to remove excessive liquid stuck to the core surface. The slices were placed in the Amott cell with the plastic spacers in between. The Amott cells were completely filled with low-salinity water, sealed and stored at the desired temperature.

The Amott cells were then left to spontaneously imbibe until oil production ceased at the given temperature. The amount of oil that had been produced was monitored daily when the oil production started to decrease. The cumulative produced oil volumes of each sample in low-salinity water ($\Delta V_{LS,i}$ where $i = A, B, C, D$) were recorded.

### 4.2.5 Core Cleaning

After each experiment was completed, the core samples were cleaned by Soxhlet extraction using methanol. The cores were left to clean in the extractor for approximately $4$ hours. After cleaning had completed the cores were dried in an oven at $50^oC$ overnight. At this point, the cores were considered ready for repeated experiments.

Chapter 5

# Results

## 5.1 Core Measurements

Two Bentheimer sandstone cores were treated using the procedure described in Section 4.1.1. The cores were standard $1.5$" diameter core plugs with lengths $69.3\ mm$ and $47.3\ mm$. The plugs were cut into smaller slices in order to obtain four core samples with varying surface-to-volume ratios. A schematic showing how the samples were cut is given in Figure 5.1.

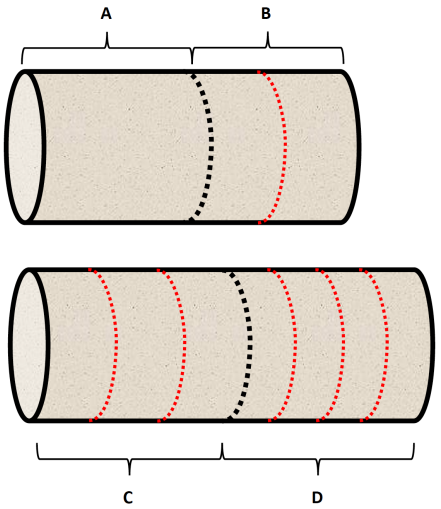


**Figure 5.1:** Schematic of how the core samples were cut from the initial core plugs. Sample B, C and D consist of multiple core slices.

Some minor imperfections could be observed on some of the cut surfaces and edges. Dust from the cutting process was removed by rinsing the cores with distilled water three times. The cores were dried in an oven at $40^oC$ for 11 days while the setup for the experiments was prepared.

## Bulk Volumes and Surface Areas

Based on the core slices' average diameter ($d_i$) and thickness ($z_i$) the samples' total bulk volumes and surface areas were calculated using Eq. 4.1 and Eq. 4.2, respectively. The volumes and areas are presented in Table 5.1. A complete list of measurements of core slice thicknesses and diameters is presented in Appendix A.

**Table 5.1:** Calculated sample bulk volumes and surface area.

| **Sample, i** | **Bulk Volume** $[cm^3]$ $\mathbf{V_{bulk}}$ | **Surface Area** $[cm^2]$ **A** |
|---|---|---|
| **A** | 27.8 | 51.9 |
| **B** | 23.5 | 69.8 |
| **C** | 43.4 | 113.3 |
| **D** | 22.8 | 114.0 |

## Pore Volumes and Porosities

Based on averages of the chamber volumes with the core sample ($V_1$) and without the sample ($V_2$), the samples' total grain volumes, pore volumes, and effective porosities were calculated using Eq. 4.3, Eq. 4.4 and eq. 4.5, respectively. The volumes and porosities are presented in Table 5.2. A complete list of volume measurements from helium porosimetry is presented in Appendix B.

**Table 5.2:** Calculated sample grain volumes, pore volumes and effective porosities.

| **Sample, i** | $\mathbf{V_{grain}}$ $[cm^3]$ | $\mathbf{V_{pore}}$ $[cm^3]$ | $\phi_\mathbf{e}$ $[-]$ |
|---|---|---|---|
| **A** | 21.2 | 6.7 | 0.24 |
| **B** | 17.8 | 5.7 | 0.24 |
| **C** | 34.0 | 9.4 | 0.22 |
| **D** | 17.2 | 5.5 | 0.24 |

## Surface-to-Volume Ratios

The calculated surface area-to-pore volume ratios are presented in Table 5.3. Figure 5.2 shows a plot of the surface areas versus pore volumes.

**Table 5.3:** Surface area to pore volume ratios.

| Sample, i | Surface-to-Volume Ratio [$cm^{-1}$] $\mathbf{A/V_{pore}}$ |
|---|---|
| **A** | 7.8 |
| **B** | 12.2 |
| **C** | 12.1 |
| **D** | 20.6 |

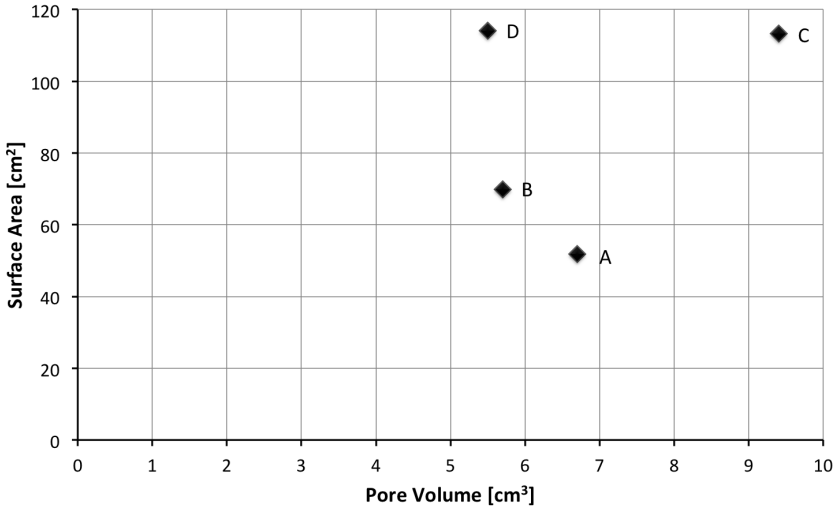


**Figure 5.2:** Plot of surface areas vs. pore volumes.

Samples C and D have similar pore volumes, samples B and C have similar surface-to-volume ratios, and samples C and D have similar surface areas. These similarities should enable us to investigate whether increased oil production is sensitive to pore volume, surface-to-volume ratio, surface area, or none.

## 5.2 Experiment at Elevated Temperature

### Water Saturation and Toluene-Flooding

The high-salinity brine ($5.0 \frac{mol}{l}$ NaCl solution) was prepared by dissolving $584.00\ g$ $NaCl$ in distilled water so that the total solution volume was $2.0\ l$. The solution was stirred for 1 hour using a magnetic stirrer. The solution is equivalent of $292,200\ ppm$. The core samples were saturated with brine using a vacuum pump. The cores were kept submerged in brine for approximately 24 hours before being flooded with toluene.

The core slices were assembled and inserted into the core holder. When applying sleeve pressure the rubber sleeve punctured. Upon inspection of the core holder, it was found that the inlet end piece was loose, indicating a cavity between the inlet and core. It was concluded that the cavity was the cause of the sleeve puncture. Visual inspection of the core slices did not reveal any damage. The cores were submerged in brine again and the rubber sleeve was replaced.

For the second attempt, the core slices were assembled, inserted into the core holder, secured between the inlet and outlet end pieces, and sleeve pressure was applied successfully. The core was flooded at $7.0\ \frac{ml}{min}$ for 20 minutes, equivalent to approximately $5.1$ pore volumes ($PV$), followed by a bump rate of $8.33\ \frac{ml}{min}$ for 12 minutes, approximately $3.7\ PV$. Visual inspection of the effluent produced from bump rate flooding showed that only a small droplet of water had been produced. In total, $13\ ml$ of water was displaced from the cores and filter paper during toluene-flooding. The cores were removed from the core holder and submerged in toluene immediately after flooding.

### High-Salinity Spontaneous Imbibition

Four Amott cells were filled with toluene-saturated high-salinity brine. The core slices were removed from the toluene, shaken firmly three times and placed in the Amott cell along with the plastic spacers. The Amott cells were filled completely with brine, sealed and placed in an oven at $70^oC$. Some toluene was released from the surface of the core when being inserted into the Amott cell.

When returning to inspect the samples after two days, brine had leaked from all of the Amott cells, but the samples were still completely submerged in brine (see Figure 5.3a). Salt crystallization was observed on the outside of the Amott cell and around the cover and gasket as shown in Figure 5.3b.

The water level in the Amott cell containing sample A had dropped below the measure graduations on the neck of the cell. It was therefore decided to refill cell A with brine. During refilling, the produced toluene evaporated without being measured. To ensure that leaks would not reoccur, high-salinity brine was heated to approximately $40^oC$ before refilling the cell and an air bubble of $2-3\ ml$ was left to account for thermal expansion. Crystallized salt was removed from the Amott cell and the cell was placed back in the oven at $70^oC$.

The water levels in the Amott cells containing sample B, C and D had dropped but were still sufficient to read the amount of produced toluene. Crystallized salt was removed from the remaining Amott cells without breaking the seals. The sealing mechanisms were tightened and cells were placed back in the oven at $70^oC$.

The samples were left to spontaneous imbibe in high-salinity brine until the volumes of produced toluene had stabilized. Oil production had stabilized after 22 days. Some of the samples had toluene droplets stuck to the core surface, the glass surface and/or the surface of the plastic spacers. To release these droplets from the surfaces, the cells were very carefully tilted or rotated before reading the amounts of produced toluene ($\Delta V_{HS,i}$). The readings were done while the system was still at elevated temperature. Toluene still stuck to surfaces was disregarded; only the toluene that had accumulated at in the neck of the Amott cell was recorded. The measurements are presented in Table 5.4.

When the Amott cells were removed from the heating cabinet and placed at ambient conditions, gas bubbles were released from the surface of the cores in sample C and the water levels in all cells decreased during cooling. At this point, the fluid levels in the cells had fallen below the measurement graduations.

## Low-Salinity Spontaneous Imbibition

The contents of the Amott cells were emptied into beakers, the cells were cleaned and filled with lukewarm ($\approx 40^oC$) toluene-saturated low-salinity water (distilled water). The core slices were lifted out of the brine, shaken firmly three times to remove excess liquid and placed in the Amott cell along with the plastic spacers. The Amott cells filled with low-salinity water until there was $2-3\ ml$ air left in the cell to account for thermal expansion. The cell was sealed and placed back in an oven at $70^oC$.

When returning to inspect the samples the next days, small amounts of brine had leaked from all of the Amott cells. There had been a decrease in water level and some salt crystallization on the outside of all the Amott cells. The water level in cell B had dropped below the measurement graduations and had to be refilled. There was a red toluene film on top of the water that evaporated during refilling without being measured. After refilling cell B the water was cloudy for more than 3 hours before becoming transparent again.

In an effort to prevent further leaks, the Amott cells were suspended upside down, pointing the cover upwards. This effectively stopped the cells from leaking, but also prevented monitoring of the amounts of produced toluene.

The samples were left to spontaneously imbibe in low-salinity water for 7 days. The cells were turned back so that the produced toluene could accumulate at the top of the Amott cell. To release these droplets from the surfaces, the cells were carefully tilted or rotated before reading the amounts of produced toluene ($\Delta V_{LS,i}$). The amount of produced toluene was recorded while the system was still at elevated temperature. The measurements are included in Table 5.4.

When the Amott cells were removed from the heating cabinet and placed at ambient conditions, gas bubbles were released from the surface of the cores in sample A and C and the

water levels in all cells decreased during cooling. At this point, the fluid levels in the cells had fallen below the measurement graduations.

**Table 5.4:** Oil production from high-salinity and low-salinity spontaneous imbibition at $70^oC$. Readings were made at elevated temperature ($70^oC$). **Additional uncertainty due to evaporation of toluene during refilling of the Amott cells.*

| Sample, i | $\Delta V_{HS,i}$ [$cm^3$] | $\Delta V_{LS,i}$ [$cm^3$] |
|---|---|---|
| **A** | 0.1* | 0.1 |
| **B** | 0.4 | 0.2* |
| **C** | 1.7 | 0.2 |
| **D** | 0.1 | 0.2 |

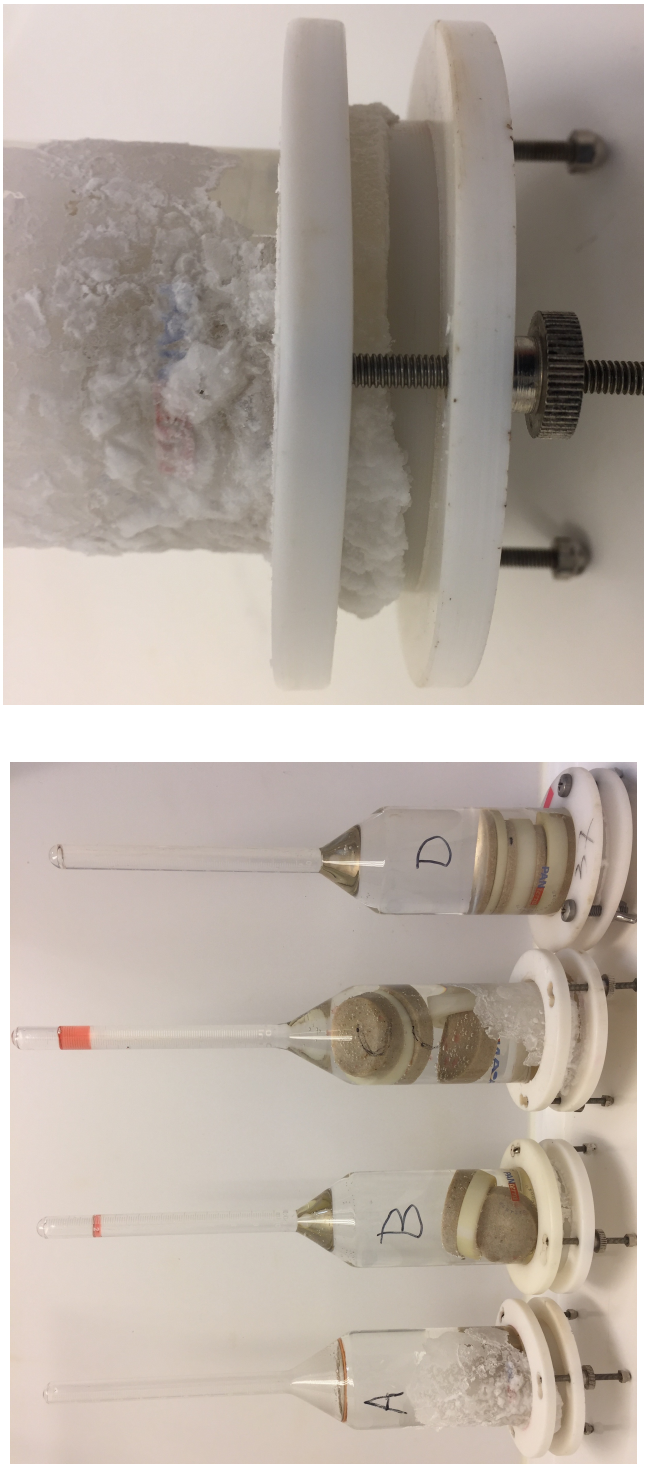


**(a)** Decrease in water level.

**(b)** Salt crystallization.

**Figure 5.3:** Decrease in water levels and salt crystallization after 2 days of high-salinity spontaneous imbibition.

## 5.3 Experiment at Ambient Temperature

After the experiments conducted at elevated temperatures, a similar experimental procedure was conducted at ambient temperature.

### Core Cleaning

The cores were cleaned using Soxhlet extraction with methanol. The cores were repeatedly rinsed in the Soxhlet for four hours and dried overnight at $50^oC$. Some red coloring was seen on the core surface after drying.

### Water Saturation and Toluene-Flooding

A new $2\ l$ batch of high-salinity brine was mixed and the cores were saturated using a vacuum pump. The cores were submerged in brine for 3 hours before the core slices were assembled and flooded with toluene. The cores were flooded at $7.0\ \frac{ml}{min}$ for 17 minutes, equivalent to approximately $4.4\ PV$, followed by $8.33\ \frac{ml}{min}$ for 8 minutes, approximately $2.4\ PV$. Visual inspection of the effluent produced from the last minute of flooding showed that no water was produced. In total, $19.8\ ml$ of water was displaced from the cores and filter paper during toluene-flooding. The cores were immediately removed from the core holder and submerged in toluene.

### High-Salinity Spontaneous Imbibition

Four Amott cells were filled with toluene-saturated high-salinity brine, the core slices removed from the toluene, shaken firmly five times and placed in the Amott cell along with the plastic spacers. The Amott cells were filled completely with brine, sealed and placed in a fume hood at room temperature ($\approx 22^oC$). Some toluene was released from the surface of the cores during insertion into the Amott cell.

The cores were left to spontaneously imbibe in high-salinity water for 20 days. The samples were monitored daily until the oil production had ceased. The Amott cells were in some cases carefully tipped to release displaced toluene that had become stuck to surfaces of the cores, plastic or glass. The amounts of toluene produced after the samples had stabilized presented in Table 5.5.

### Low-Salinity Spontaneous Imbibition

The contents of the Amott cells were emptied into beakers, the cells were cleaned and filled with toluene-saturated low-salinity water (distilled water). The core slices were lifted out of the brine, shaken firmly ten times to remove excess liquid and placed in the Amott cell

along with the plastic spacers. The Amott cells were completely filled with low-salinity water, sealed and placed at room temperature in a fume hood.

After imbibing for five days, during an inspection of the samples, the Amott cell containing sample C tipped and broke. Fortunately, the amount of produced toluene was recorded moments before breaking the cell and only small amounts of water had managed to leak out of the cell. The sample and remaining fluids were immediately moved to a new Amott cell, exposing the core sample to air for less than 30 seconds. The cell was applied $10\ ml$ toluene-saturated low-salinity water to ensure that the water level was high enough and the cell was sealed. At this point, $0.4\ ml$ toluene had leaked out of the cell. The amount of produced toluene in proceeding readings was corrected adding this loss.

The samples were left to spontaneously imbibe in low-salinity water for $21$ days in total. The samples were monitored daily until the toluene production had ceased. The amounts of produced toluene versus time are presented in Figure 5.4. The final measurements are presented in Table 5.5.

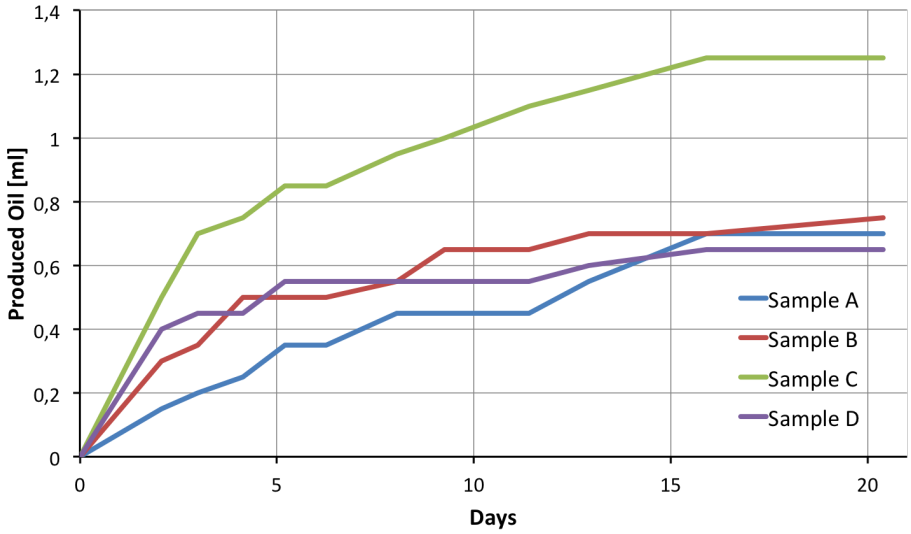


**Figure 5.4:** Produced oil vs. time for low-salinity spontaneous imbibition at ambient temperature.

**Table 5.5:** Oil production from high-salinity and low-salinity spontaneous imbibition at ambient temperature. **Additional uncertainty associated with measurement due to change of Amott cell during the experiment.*

| Sample, i | $\Delta V_{HS,i}$ [$cm^3$] | $\Delta V_{LS,i}$ [$cm^3$] |
|---|---|---|
| **A** | 0.15 | 0.7 |
| **B** | 0.15 | 0.7 |
| **C** | 0.35 | 1.25* |
| **D** | 0.4 | 0.65 |

Chapter 6

# Discussion

In this section, we will first discuss some effects related to the experimental procedure and how the experimental design is expected to promote osmosis while impeding other proposed low-salinity mechanisms. Further, we will investigate the results of the experiments in light of osmosis.

## 6.1 Procedure-Related Effects

### Thermal Effects

Fluid preparations, water and toluene saturation of the cores and assembling of the Amott cells was performed at ambient temperature. The samples used in the experiment at $70^oC$ were, therefore, subject to repeated heating and cooling. The effects of thermal expansion on oil production and the temperature dependency of toluene in water solubility must, therefore, be taken into consideration.

Both high-salinity and low-salinity water solutions were toluene-saturated before being used in the Amott cells. The solubility of toluene in water is temperature dependent and increases with increasing temperature above $291\ K$ [42]. Heating the water solutions while dissolution of toluene was done to reduce the amount of toluene being dissolved during the experiment. However, the solutions were closer to room temperature than $70^oC$ during assembly of the Amott cells and dissolution of toluene is likely to have occurreda after the experiments were initiated. The toluene solubility in water, given as liquid mole fraction, is $1.2 \cdot 10^{-4}$ at $25^oC$ and $1.8 \cdot 10^{-4}$ at $70^oC$ [42]. The volume of an Amott cells is $250\ ml$. An increase in temperature from $25^oC$ to $70^oC$ would enable approximately $0.9\ ml$ additional toluene to dissolve in the water.

For the first experiment, the Amott cells had been prepared at room temperature and then heated to $70^oC$. During heating, the cells started leaking causing the water levels to decrease and salt to crystallize on the outside of the cell. The water leaks are believed to be caused by a combination of temperature-related issues. The plastic locking mechanism had become more ductile after heating, preventing proper sealing. In addition, the cells were almost completely filled with water at room temperature before being place in the oven. Thermal expansion may have applied a high pressure on the lid, causing it to be pushed open and enabling water to leak from the cell. Salt crystallization observed between the glass cell and the lid from evaporation of the leaked water is believed to have prevented re-sealing of the cell when the pressure decreased.

The thermal expansion coefficients for toluene and water at $25^oC$ are $0.00108\ K^{-1}$ and $0.000214\ K^{-1}$ respectively [44]. An increase in temperature from $25^oC$ to $70^oC$ will cause toluene and water to expand approximately $5\%$ and $1\%$, respectively. This implies that thermal expansion of water in the Amott cell caused a volumetric increase of approximately $2.5\ ml$, which should be enough to explain the occurrence of leaks.

Thermal expansion may have caused displacement of fluids from the core and could represent a significant source of error. Thermal expansion may also have affected the fluid distribution in the cores. One possible effect is expansion of encapsulated connate water causing the oil membranes to rupture and effectively eliminating the potential for osmosis-induced connate water expansion.

## Coreflooding End Effects

Because toluene-flooding was performed on an assembly of small core slices, end effects may constitute a significant source of error for the experiment with regard to the initial saturation profile. In case of end effects, irregularities in the initial saturation profile would be much more significant for the small core slices than the larger slices. During toluene-flooding, filter papers were used to establish capillary continuity between the core slices in an effort to restrict end effects. It is, however, uncertain if establishing capillary continuity was successful.

End effects may be experienced at both the inlet and outlet of solid cores during coreflooding experiments. Kyte and Rapoport (1958) discussed end effects for waterflooding in water-wet cores initially saturated with oil [45]. They argued that spontaneous imbibition may cause water to imbibe into the core near the inlet, thereby causing a local increase in water saturation. They also argued that a discontinuity in capillary pressure at the outlet may cause a local increase in water saturation.

In our experiment, the situation is similar to the one described by Kyte and Rapoport (1958), except oil is the wetting phase while water is the non-wetting phase. Toluene is flooded through an oil-wet core which is initially saturated with water, i.e. the core is initially saturated with the non-wetting phase and is flooded by the wetting phase. Using the same analogy as Kyte and Rapoport (1958), toluene-flooding is expected to locally increase the oil saturation near both the inlet and outlet.

The end effects are expected to be most pronounced during the transient flow period. However, because wettability and toluene-flooding both act to increase oil saturation towards the residual oil saturation ($S_{or}$), the end effects are not expected to have any significant effect on the saturation profile after the transient period. The same argument could be made independent of whether capillary continuity is successfully established or not.

## 6.2 Isolation of the Osmosis Mechanism

The spontaneous imbibition experiment performed here was designed to facilitate osmosis while mitigating or eliminating other proposed low-salinity mechanisms.

Spontaneous imbibition experiments are assumed to effectively eliminate low-salinity mechanisms related to viscous flow such as fines migration. In addition, Bentheimer has a low clay content (typically less than $5\%$ [41]) and the silane treatment used to render the sandstone samples oil-wet is a surface altering treatment which is performed at high temperatures ($95 - 100^oC$), and is, therefore, believed to mitigate or eliminate the effects of destabilization of solids and clay swelling.

The total water volume in the Amott cells ($250\ ml$) is much larger than the sample volume (maximum $9.6\ ml$). Any $OH^-$ generated by reactions between low-salinity water and mineral in the core should diffuse along continuous water paths, eventually exiting the core. Because of the difference in volume, this process should continuously dilute the $OH^-$ concentration in the core and prevent any significant changes in pH.

The silane treatment rendering the core strongly oil-wet is expected to reduce the sensitivity of increased oil production to small wettability alterations. If the wettability is altered slightly towards more water-wet, oil will still remain the dominant wetting phase. In addition, the use of refined oil without organic polar compounds should also work to eliminate the wettability alteration mechanism.

## 6.3 Spontaneous Imbibition Results

A comparison of oil produced by high-salinity and low-salinity experiments is presented in Figure 6.1. The amounts of produced oil during high-salinity spontaneous imbibition are generally low, indicating that the core samples are highly oil-wet. Comparing the results of the experiments it is apparent that the experiment at elevated temperature had a higher response to high-salinity spontaneous imbibition than low-salinity spontaneous imbibition. Contrarily, the experiment at ambient temperature had a higher response to low-salinity imbibition. The amount oil produced from high-salinity spontaneous imbibition at ambient temperature is also low, indicating that the cleaning procedure did not reverse the effect of the silane surface treatment.

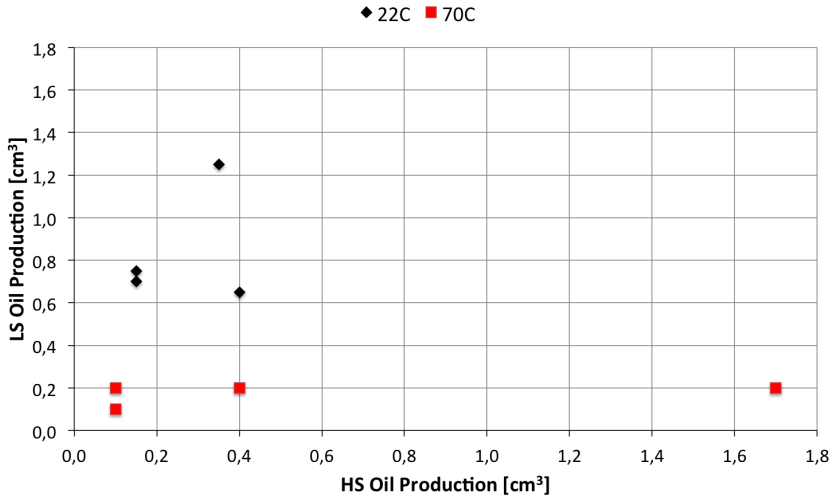


**Figure 6.1:** Increased oil production by low-salinity spontaneous imbibition vs. oil production by high-salinity spontaneous imbibition.

The measurement graduations on the Amott cells are marked in $0.1\ ml$ intervals, meaning that the associated visual measurement error in the order of $\pm 0.05\ ml$. Due to small high-salinity response, the significance of the measurement uncertainty is too large to make reasonable inferences about trends of oil production data from the high-salinity spontaneous imbibition experiments. The low-salinity responses from the experiment at elevated temperature are also considered to be too small to make reasonable inferences from this data. It is also likely that temperature-related effects from repeated temperature changes have obstructed the results of both high-salinity and low-salinity spontaneous imbibition. For these reasons, the focus of this discussion will be on the increased oil recovery from low-salinity spontaneous imbibition at ambient temperature.

In Section 2.3, it was argued that osmotic oil relocation would yield a linear relationship between increased oil production ($\Delta V_{LS,oil}$) and surface area ($A$). Figure 6.2 shows a plot of $\Delta V_{LS,oil}$ versus $A$. The results fail to show any clear linear relation.

Oil recovery is expected to be proportional to $\frac{\Delta V_{LS,oil}}{V_{pore}}$. Therefore, a plot of oil recovery versus the surface-to-volume ratio would exhibit the same behavior as seen in Figure 6.2. Hence, the results of these experiments do not show any correlation between increased oil recovery and surface-to-volume ratio. This limits further discussions of the relative importance of osmosis in low-salinity experimental results.

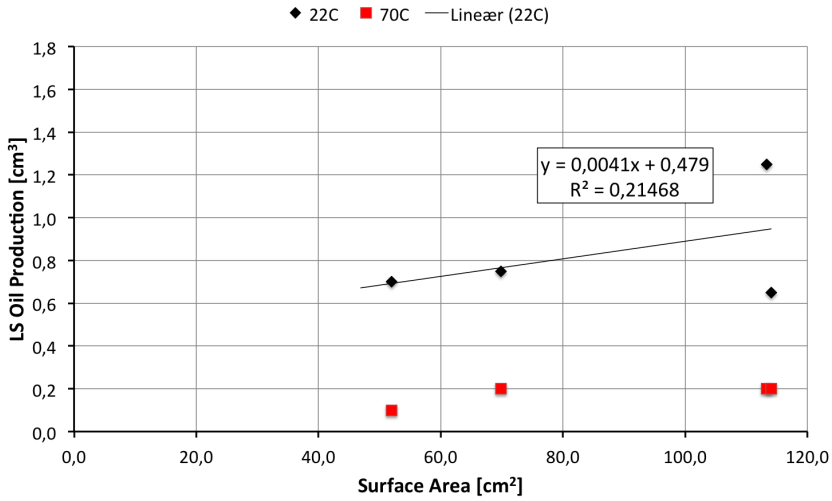


**Figure 6.2:** Increased oil production from low-salinity spontaneous imbibition vs. surface area.

Figure 6.3 shows increased oil production per pore volume ($\frac{\Delta V_{LS,oil}}{V_{pore}}$) versus surface area ($A$). There is no clear trend; however, the largest oil recoveries are from the samples with high surface area, but there are large variations in oil recovery for samples with similar surface areas.

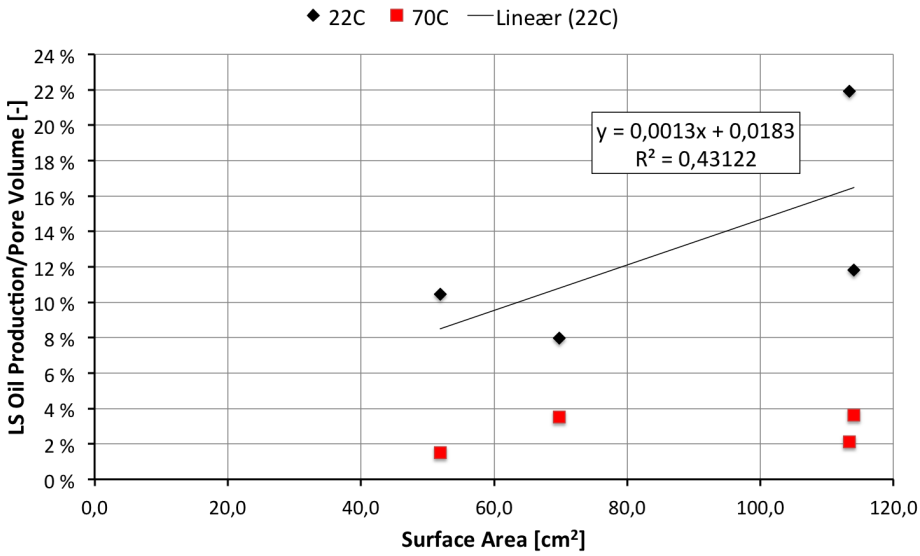


**Figure 6.3:** Increased oil production from low-salinity spontaneous imbibition per pore volume vs. surface area.

The results of the experiment also fail to show any relationship between increased oil recovery ($\Delta V_{LS,oil}$) and the surface-to-volume ratio ($\frac{A}{V_{pore}}$) as presented in Figure 6.4.

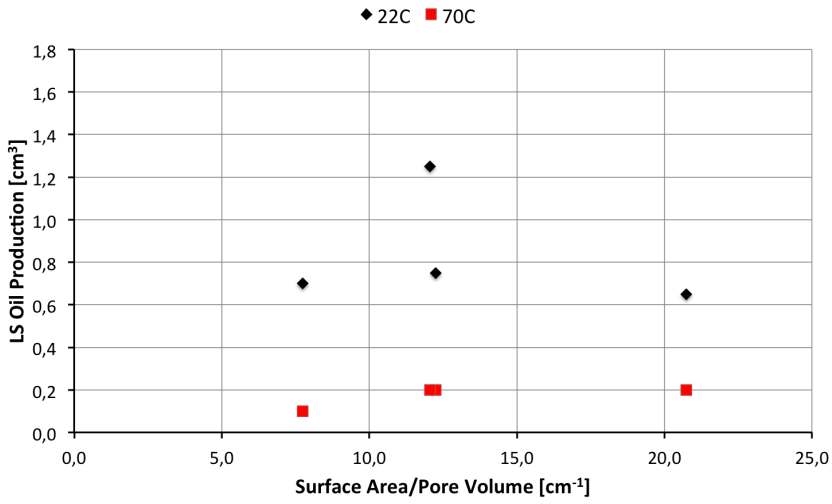


**Figure 6.4:** Increased oil production from low-salinity spontaneous imbibition vs. surface-to-volume ratio.

Figure 6.5 shows a plot of $\Delta V_{LS,oil}$ versus $V_{pore}$. For the experiment at ambient temperature, there seems to be a linear relationship between increased oil production and pore volume. The uncertainty associated with the measurement gives a fair approximation for the trend of the measured data to intersect at the origin.

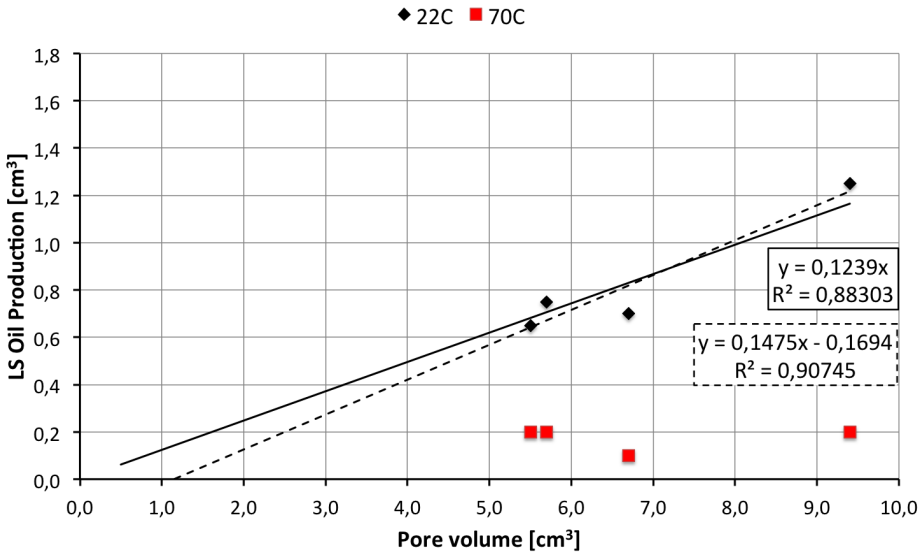


**Figure 6.5:** Increased oil production from low-salinity spontaneous imbibition vs. pore volume.

## 6.4 Osmotic Oil Production and Pore Volume

A linear relation between increased oil recovery and pore volume could be expected by several other low-salinity mechanisms such as wettability alteration. However, both the oil-wet regime and the use of refined oil should mitigate the wettability alteration effect. Hence, it seems unlikely that wettability alteration is the cause of this response.

The osmotic oil relocation phenomenon used to argue that there should be a linear relationship between increased oil recovery and surface area in Section 2.3 assumes that connate water expansion causes a corresponding invading water shrinkage. A schematic of oil relocation by corresponding water expansion and shrinkage is shown in Figure 6.6a.

There are two main diffusion processes occurring during the low-salinity spontaneous imbibition; diffusion of dissolved salt along continuous water paths and osmotic water transport through oil. If the time needed for salt to diffuse through the core is much less than the time needed for connate water expansion to occur, expansion may occur approximately simultaneously throughout the core sample. Capillary forces may then act more strongly on the low-salinity invading water due to the low water saturation and impair shrinkage

of the invading water. This is possible if water outside the core continuously imbibes into the core at the same rate as osmotic water transport passes water to the high-salinity water. Connate water expansion will then force oil to flow along the continuous oil films towards the core surface. A schematic of osmotic oil relocation by film flow is shown in Figure 6.6b. If connate water expansion occur throughout the core, increased oil production should be proportional to the pore volume.

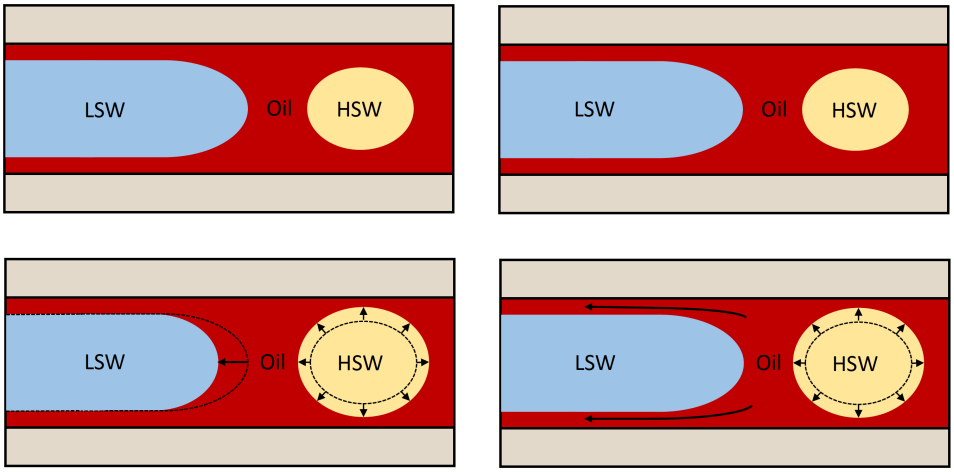


**(a)** Connate water expansion and corresponding invading water shrinkage causing the LSW/oil interface to retreat.

**(b)** Connate water expansion without corresponding invading water shrinkage causing oil film flow.

**Figure 6.6:** Schematic of osmotic oil relocation at pore scale. LSW = low-salinity water (invading water), HSW = high-salinity water (connate water).

In Section 4.1.2, it was estimated that it would take 3 days for the dissolved salt to diffuse out of the biggest cores after being placed in distilled water. This was considered to be a conservative estimate. In the visualization experiment performed by Sandengen et al. (2016) on an oil-wet Bentheimer sandstone plug with 5 $mm$ diameter (see Figure 2.21), connate water expansion had initiated throughout the core within the first 7 hours. Hence, the time needed for salt to diffuse out of the core is seemingly not significantly faster than connate water expansion. However, these cases use cores with different sizes and, therefore, requires further investigation.

Hysteresis effects is another possible explanation of the linear relation increased oil recovery and pore volume. Hysteresis effects are a result of capillary pressure being a function of more than just water saturation, e.g. fluid distribution. The effect is illustrated in Figure 6.7. Assume that a core is initially saturated with oil and water at irreducible water saturation, $S_{wir}$. During high-salinity spontaneous imbibition, water will imbibe into the core spontaneously (point 1 to 2). If salt diffusion time is not significantly faster than osmotic water transport, connate water expansion during low-salinity spontaneous imbibition will occur near the core surface first. Here, the pressure will build up in the encapsulated connate water, eventually forcing imbibition (point 2 to 3). Connate water expansion fur-

ther inside the core may later invert the process near the core surface from imbibition to drainage due to oil moving outwards. The capillary pressure will follow the drainage scanning curves (see Figure 6.7a) towards a lower saturation (point 3 to 4). When connate water expansion ceases, the drainage process stops and spontaneous imbibition will drive oil production until the fluid system is back at equilibrium (point 4 to 5 in Figure 6.7b). As we can see, hysteresis effects cause higher and more favorable water saturation than after the initial high-salinity spontaneous imbibition test.

Simplified, hysteresis allows oil to pass more easily from the center through the core, towards the core surface. Hysteresis would imply a correlation between oil production and the pore volume of the sample.

Initially, it was assumed that osmosis was a surface effect that would result in a linear relationship between increased oil production and surface area. This was not observed. Contrarily, there are indications of a linear relationship between increased oil production and pore volume. This result does not reject osmosis as a low-salinity mechanism, but a re-investigation of osmotic oil relocation might be necessary to understand the phenomenon. Two explanations have been suggested for how osmosis relates to pore volume, but more work is necessary to verify or reject these. In addition, more measurements are needed to conclude with certainty whether there is a linear relationship between $\Delta V_{LS,oil}$ and $A$, or $\Delta V_{LS,oil}$ and $V_{pore}$.

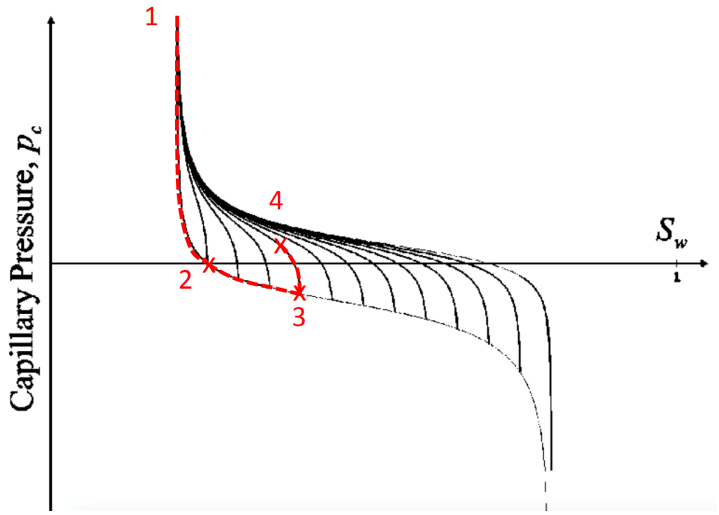


**(a)** Drainage scanning curves. Spontaneous imbibition (1 to 2), and forced imbibition (2 to 3), followed by drainage (3 to 4).

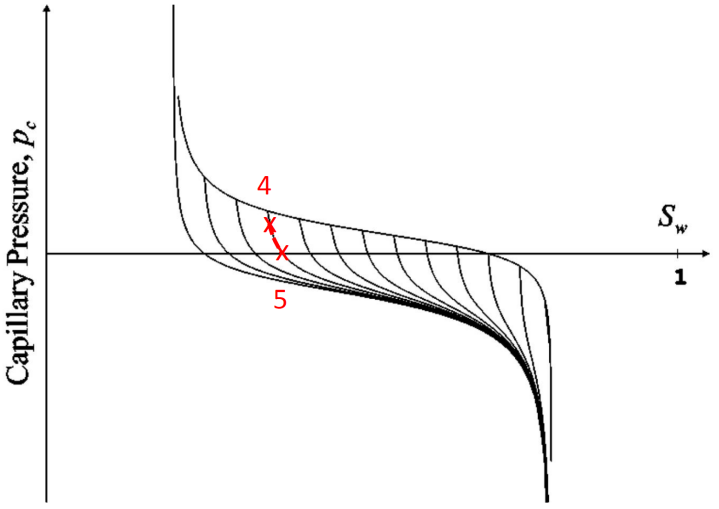


**(b)** Imbibition scanning curves. Spontaneous imbibition (4 to 5).

**Figure 6.7:** Illustration of hysteresis effect and how it yields favourable water saturation. [46]

Chapter 7

# Conclusions

The aim of this thesis was to evaluate the relative importance of osmosis as a low-salinity mechanism. The foundation of the experimental investigation was that oil recovery due to osmosis was expected to have a stronger correlation to the surface-to-volume ratio than other proposed low-salinity mechanisms. The main findings of this investigation are:

- The results of the low-salinity spontaneous imbibition experiment do not show any clear correlation between increased oil recovery and the surface-to-volume ratio.
- The results of the experiment do indicate a correlation between increased oil production and pore volume.
- The investigation was unsuccessful in evaluating the relative importance of osmosis as a low-salinity mechanism.
- The outcome the investigation does not contradict osmosis as a low-salinity mechanism.

Chapter 8

# Suggestions of Further Work

For further work, it is suggested that more low-salinity spontaneous imbibition experiments be performed on core samples with varying surfaces areas to determine if increased oil recovery due to osmosis relates to the surface-to-volume ratio. It is suggested to perform low-salinity spontaneous imbibition experiments on large core samples to prevent simultaneous connate water expansion throughout the core.

It is also suggested to investigate how connate water expansion displaces oil during low-salinity spontaneous imbibition experiments. A simple visualization experiment may be performed for this purpose by submerging oil-wet micromodels in low-salinity water, without any induced pressure difference over the sample.

# Bibliography


[1] Norman Morrow and Jill Buckley. Improved Oil Recovery by Low-Salinity Waterflooding. *SPE-129421-JPT*, May 2011. doi: 10.2118/129421-JPT.

[2] Bart Suijkerbuijk, Jan Hofman, Dick Jacob Ligthelm, Julija Romanuka, Niels Brussee, Hilbert van der Linde, and Fons Marcelis. Fundamental Investigations into Wettability and Low Salinity Flooding by Parameter Isolation. In *SPE-154204-MS*, SPE, January 2012. Society of Petroleum Engineers. ISBN 978-1-61399-197-8. doi: 10.2118/154204-MS.

[3] P.L. McGuire, J.R. Chatham, F.K. Paskvan, D.M. Sommer, and F.H. Carini. Low Salinity Oil Recovery: An Exciting New EOR Opportunity for Alaska's North Slope. In *SPE-93903-MS*, SPE, January 2005. Society of Petroleum Engineers. ISBN 978-1-61399-013-1. doi: 10.2118/93903-MS.

[4] Pudji P. Jadhunandan. *Effects of brine composition, crude oil, and aging conditions on wettability and oil recovery*. PhD thesis, New Mexico Institute of Mining & Technology, Department of Petroleum Engineering, 1990.

[5] G.Q. Tang and N.R. Morrow. Salinity, Temperature, Oil Composition, and Oil Recovery by Waterflooding. *SPE-36680-PA*, November 1997. doi: 10.2118/36680-PA.

[6] Ma Shouxiang, Norman R. Morrow, and Xiaoyun Zhang. Generalized scaling of spontaneous imbibition data for strongly water-wet systems. *Journal of Petroleum Science and Engineering*, 18(3):165–178, November 1997. ISSN 0920-4105. doi: 10.1016/S0920-4105(97)00020-X. URL `http://www.sciencedirect.com/science/article/pii/S092041059700020X`.

[7] K.J. Webb, C.J.J. Black, and H. Al-Ajeel. Low Salinity Oil Recovery - Log-Inject-Log. In *SPE-89379-MS*, SPE, January 2004. Society of Petroleum Engineers. ISBN 978-1-55563-988-4. doi: 10.2118/89379-MS.

[8] Arnaud Lager, Kevin John Webb, Ian Ralph Collins, and Diane Marie Richmond. LoSal Enhanced Oil Recovery: Evidence of Enhanced Oil Recovery at the Reservoir

Scale. In *SPE-113976-MS*, SPE, January 2008. Society of Petroleum Engineers. ISBN 978-1-55563-225-0. doi: 10.2118/113976-MS.

[9] Jim Seccombe, Arnaud Lager, Gary Jerauld, Bharat Jhaveri, Todd Buikema, Sierra Bassler, John Denis, Kevin Webb, Andrew Cockin, and Esther Fueg. Demonstration of Low-Salinity EOR at Interwell Scale, Endicott Field, Alaska. In *SPE-129692-MS*, SPE, January 2010. Society of Petroleum Engineers. ISBN 978-1-55563-289-2. doi: 10.2118/129692-MS.

[10] Kjetil Skrettingland, Torleif Holt, Medad Twimukye Tweheyo, and Ingun Skjevrak. Snorre Low Salinity Water Injection - Core Flooding Experiments And Single Well Field Pilot. In *SPE-129877-MS*, SPE, January 2010. Society of Petroleum Engineers. ISBN 978-1-55563-289-2. doi: 10.2118/129877-MS.

[11] James J. Sheng. *Modern Chemical Enhanced Oil Recovery - Theory and Practice*. Elsevier Science, October 2010. ISBN 978-1-85617-745-0. URL http://app.knovel.com/hotlink/toc/id:kpMCEORTP2/modern-chemical-enhanced/modern-chemical-enhanced.

[12] Christopher E. Reddick, Todd Alan Buikema, and Dale Williams. Managing Risk in the Deployment of New Technology: Getting LoSal into the Business. In *SPE-153933-MS*, SPE, January 2012. Society of Petroleum Engineers. ISBN 978-1-61399-197-8. doi: 10.2118/153933-MS.

[13] Enis Robbana, Todd Alan Buikema, Christopher Mair, Dale Williams, David James Mercer, Kevin John Webb, Aubrey Hewson, and Christopher E. Reddick. Low Salinity Enhanced Oil Recovery - Laboratory to Day One Field Implementation - LoSal EOR into the Clair Ridge Project. In *SPE-161750-MS*, SPE, January 2012. Society of Petroleum Engineers. ISBN 978-1-61399-217-3. doi: 10.2118/161750-MS.

[14] Low salinity water brings award for BP | Innovations | BP Magazine | BP Global, . URL http://www.bp.com/en/global/corporate/bp-magazine/innovations/offshore-technology-award-for-clair-ridge.html.

[15] Clair Ridge | North Sea major projects | North Sea | Where we operate | United Kingdom, . URL http://www.bp.com/en_gb/united-kingdom/where-we-operate/north-sea/north-sea-major-projects/clair-ridge.html.

[16] I. R. Collins. Holistic Benefits of Low Salinity Waterflooding. Cambridge, United Kingdom, April 2011. EAGE. doi: 10.3997/2214-4609.201404797.

[17] Guo-Qing Tang and Norman R Morrow. Influence of brine composition and fines migration on crude oil/brine/rock interactions and oil recovery. *Journal of Petroleum Science and Engineering*, 24(2–4):99–111, December 1999. ISSN 0920-4105. doi: 10.1016/S0920-4105(99)00034-0. URL http://www.sciencedirect.com/science/article/pii/S0920410599000340.

[18] Shouxiang Ma and N.R. Morrow. Effect of Firing on Petrophysical Properties of Berea Sandstone. *SPE-21045-PA*, September 1994. doi: 10.2118/21045-PA.

[19] M. Sohrabi, P. Mahzari, S. A. Farzaneh, J. R. Mills, P. Tsolis, and S. Ireland. Novel Insights into Mechanisms of Oil Recovery by Low Salinity Water Injection. In *SPE-172778-MS*, SPE, March 2015. Society of Petroleum Engineers. ISBN 978-1-61399-343-9. doi: 10.2118/172778-MS.

[20] R.N. Valdya and H.S. Fogler. Fines Migration and Formation Damage: Influence of pH and Ion Exchange. *SPE-19413-PA*, November 1992. doi: 10.2118/19413-PA.

[21] Yongsheng Zhang, Xina Xie, and Norman R. Morrow. Waterflood Performance By Injection Of Brine With Different Salinity For Reservoir Cores. In *SPE-109849-MS*, SPE, January 2007. Society of Petroleum Engineers. ISBN 978-1-55563-148-2. doi: 10.2118/109849-MS.

[22] Seung Yeon Lee, Kevin John Webb, Ian Collins, Arnaud Lager, Stuart Clarke, Michael O'Sullivan, Alex Routh, and Xiaofan Wang. Low Salinity Oil Recovery: Increasing Understanding of the Underlying Mechanisms. In *SPE-129722-MS*, SPE, January 2010. Society of Petroleum Engineers. ISBN 978-1-55563-289-2. doi: 10.2118/129722-MS.

[23] T. Austad, S. Strand, E.J. Høgnesen, and P. Zhang. Seawater as IOR Fluid in Fractured Chalk. In *SPE-93000-MS*, SPE, January 2005. Society of Petroleum Engineers. ISBN 978-1-61399-002-5. doi: 10.2118/93000-MS.

[24] Skule Strand, Eli J. Høgnesen, and Tor Austad. Wettability alteration of carbonates—Effects of potential determining ions (Ca2+ and SO42) and temperature. *Colloids and Surfaces A: Physicochemical and Engineering Aspects*, 275 (1–3):1–10, March 2006. ISSN 0927-7757. doi: 10.1016/j.colsurfa.2005.10.061. URL `http://www.sciencedirect.com/science/article/pii/S092777570500796X`.

[25] Peimao Zhang and Tor Austad. Wettability and oil recovery from carbonates: Effects of temperature and potential determining ions. *Colloids and Surfaces A: Physicochemical and Engineering Aspects*, 279(1–3):179–187, May 2006. ISSN 0927-7757. doi: 10.1016/j.colsurfa.2006.01.009. URL `http://www.sciencedirect.com/science/article/pii/S0927775706000148`.

[26] Peimao Zhang, Medad T. Tweheyo, and Tor Austad. Wettability alteration and improved oil recovery by spontaneous imbibition of seawater into chalk: Impact of the potential determining ions Ca2+, Mg2+, and SO42. *Colloids and Surfaces A: Physicochemical and Engineering Aspects*, 301(1–3):199–208, July 2007. ISSN 0927-7757. doi: 10.1016/j.colsurfa.2006.12.058. URL `http://www.sciencedirect.com/science/article/pii/S0927775706009915`.

[27] Julija Romanuka, Jan Hofman, Dick Jacob Ligthelm, Bart Suijkerbuijk, Fons Marcelis, Sjaam Oedai, Niels Brussee, Hilbert van der Linde, Hakan Aksulu, and Tor Austad. Low Salinity EOR in Carbonates. In *SPE-153869-MS*, SPE, Jan-

uary 2012. Society of Petroleum Engineers. ISBN 978-1-61399-197-8. doi: 10.2118/153869-MS.

[28] Skule Strand, Tor Austad, Tina Puntervold, Eli J. Høgnesen, Martin Olsen, and Sven Michael F. Barstad. "Smart Water" for Oil Recovery from Fractured Limestone: A Preliminary Study. *Energy & Fuels*, 22(5):3126–3133, September 2008. ISSN 0887-0624. doi: 10.1021/ef800062n. URL http://dx.doi.org/10.1021/ef800062n.

[29] Reyadh A. Almehaideb, Mamdouh T. Ghannam, and Abdulrazag Y. Zekri. Experimental Investigation of Contact Angles Under Oil-Microbial Solution on Carbonate Rocks. *Petroleum Science and Technology*, 22(3-4):423–438, January 2004. ISSN 1091-6466. doi: 10.1081/LFT-120024568. URL http://dx.doi.org/10.1081/LFT-120024568.

[30] Mohammed B. Alotaibi, Ramez Azmy, and Hisham A. Nasr-El-Din. Wettability Challenges in Carbonate Reservoirs. In *SPE-129972-MS*, SPE, January 2010. Society of Petroleum Engineers. ISBN 978-1-55563-289-2. doi: 10.2118/129972-MS.

[31] Ali A. Yousef, Salah Al-Saleh, Abdulaziz Ubaid Al-Kaabi, and Mohammed Saleh Al-Jawfi. Laboratory Investigation of Novel Oil Recovery Method for Carbonate Reservoirs. In *SPE-137634-MS*, SPE, January 2010. Society of Petroleum Engineers. ISBN 978-1-55563-312-7. doi: 10.2118/137634-MS.

[32] K. Sandengen and O.J. Arntzen. Osmosis During Low Salinity Water Flooding. St. Petersburg, Russia, April 2013. EAGE. doi: 10.3997/2214-4609.20142608.

[33] S. B. Fredriksen, A. U. Rognmo, K. Sandengen, and M. A. Fernø. Wettability Effects on Osmosis as an Oil-Mobilization Mechanism During Low-Salinity Waterflooding. *SPWLA-2017-v58n1a3*, February 2017.

[34] Kristian Sandengen, Anders Kristoffersen, Karen Melhuus, and Leif O. Jøsang. Osmosis as Mechanism for Low-Salinity Enhanced Oil Recovery. *SPE-179741-PA*, August 2016. doi: 10.2118/179741-PA.

[35] W.-B. Bartels, H. Mahani, S. Berg, R. Menezes, J. A. van der Hoeven, and A. Fadili. Low Salinity Flooding (LSF) in Sandstones at Pore Scale: Micro-Model Development and Investigation. In *SPE-181386-MS*, SPE, September 2016. Society of Petroleum Engineers. ISBN 978-1-61399-463-4. doi: 10.2118/181386-MS.

[36] Morten Helbæk and Signe Kjelstrup. *Fysikalsk kjemi*. Fagforlaget, Bergen, 2 edition, 2006. ISBN 978-82-450-0404-5.

[37] Carl Fredrik Berg, Anna Danilova, and Ming Liu. Upscaling of polymer adsorption. Unpublished paper, May 2017.

[38] Carl Fredrik Berg. Re-examining Archie's law: Conductance description by tortuosity and constriction. *Physical Review E*, 86(4):046314, October 2012. URL https://link.aps.org/doi/10.1103/PhysRevE.86.046314.

[39] Erwin Kreyszig. *Advanced Engineering Mathematics*. John Wiley & Sons, Asia, 10 edition, 2011. ISBN 978-0-470-64613-7. p. 558-561.

[40] Jay W. Grate, Marvin G. Warner, Jonathan W. Pittman, Karl J. Dehoff, Thomas W. Wietsma, Changyong Zhang, and Mart Oostrom. Silane modification of glass and silica surfaces to obtain equally oil-wet surfaces in glass-covered silicon micromodel applications. *Water Resources Research*, 49(8):4724–4729, 2013. ISSN 1944-7973. doi: 10.1002/wrcr.20367. URL http://dx.doi.org/10.1002/wrcr.20367.

[41] Anna E. Peksa, Karl-Heinz A.A. Wolf, and Pacelli L.J. Zitha. Bentheimer sandstone revisited for experimental purposes. *Marine and Petroleum Geology*, 67: 701–719, November 2015. ISSN 0264-8172. doi: 10.1016/j.marpetgeo.2015.06.001. URL http://www.sciencedirect.com/science/article/pii/S0264817215300106.

[42] Constantine Tsonopoulos. Thermodynamic analysis of the mutual solubilities of hydrocarbons and water. *Fluid Phase Equilibria*, 186(1–2):185–206, August 2001. ISSN 0378-3812. doi: 10.1016/S0378-3812(01)00520-9. URL http://www.sciencedirect.com/science/article/pii/S0378381201005209.

[43] Christopher J. D. Fell and H. Peter. Hutchison. Diffusion coefficients for sodium and potassium chlorides in water at elevated temperatures. *Journal of Chemical & Engineering Data*, 16(4):427–429, October 1971. ISSN 0021-9568. doi: 10.1021/je60051a005. URL http://dx.doi.org/10.1021/je60051a005.

[44] The Engineering ToolBox. Volumetric or Cubical Expansion Coefficients of Liquids. URL http://www.engineeringtoolbox.com/cubical-expansion-coefficients-d_1262.html.

[45] J.R. Kyte and L.A. Rapoport. Linear Waterflood Behavior and End Effects in Water-Wet Porous Media. *SPE-929-G*, October 1958. doi: 10.2118/929-G.

[46] S.M. Skjaeveland, L.M. Siqveland, A. Kjosavik, W.L. Hammervold Thomas, and G.A. Virnovsky. Capillary Pressure Correlation for Mixed-Wet Reservoirs. *SPE-60900-PA*, February 2000. doi: 10.2118/60900-PA.

# Appendix A

**Table 8.1:** Core measurements for sample A.

| Slice | Measurement | Diameter d [mm] | Thickness z [mm] |
|---|---|---|---|
| **1** | 1 | 37.84 | 24.69 |
| | 2 | 37.84 | 24.89 |
| | 3 | 37.84 | 24.65 |
| | **Average** | **37.84** | **24.74** |

**Table 8.2:** Core measurements for sample B

| Slice | Measurement | Diameter d [mm] | Thickness z [mm] |
|---|---|---|---|
| **1** | 1 | 37.83 | 10.55 |
| | 2 | 37.83 | 10.55 |
| | 3 | 37.83 | 10.56 |
| | **Average** | **37.83** | **10.55** |
| **2** | 1 | 37.84 | 10.36 |
| | 2 | 37.84 | 10.35 |
| | 3 | 37.83 | 10.35 |
| | **Average** | **37.84** | **10.35** |

**Table 8.3:** Core measurements for sample C

| Slice | Measurement | Diameter d [mm] | Thickness z [mm] |
|---|---|---|---|
| **1** | 1 | 37.88 | 12.25 |
| | 2 | 37.84 | 12.25 |
| | 3 | 37.84 | 12.25 |
| | **Average** | **37.85** | **12.25** |
| **2** | 1 | 37.84 | 13.08 |
| | 2 | 37.84 | 13.05 |
| | 3 | 37.84 | 13.06 |
| | **Average** | **37.84** | **13.06** |
| **3** | 1 | 37.84 | 13.23 |
| | 2 | 37.83 | 13.25 |
| | 3 | 37.85 | 13.25 |
| | **Average** | **37.84** | **13.24** |

**Table 8.4:** Core measurements for sample D

| Slice | Measurement | Diameter d [mm] | Thickness z [mm] |
|---|---|---|---|
| **1** | 1 | 37.85 | 5.15 |
| | 2 | 37.85 | 5.09 |
| | 3 | 37.85 | 5.08 |
| | **Average** | **37.85** | **5.11** |
| **2** | 1 | 37.84 | 5.00 |
| | 2 | 37.85 | 5.04 |
| | 3 | 37.84 | 5.05 |
| | **Average** | **37.84** | **5.03** |
| **3** | 1 | 37.84 | 5.03 |
| | 2 | 37.85 | 5.02 |
| | 3 | 37.84 | 5.02 |
| | **Average** | **37.84** | **5.02** |
| **4** | 1 | 37.83 | 5.07 |
| | 2 | 37.83 | 5.08 |
| | 3 | 37.84 | 5.08 |
| | **Average** | **37.83** | **5.08** |

# Appendix B

**Table 8.5:** Gas volume measurements by helium porosimeter for sample A.

| Measurement | $V_1\ [cm^3]$ | $V_2\ [cm^3]$ |
|---|---|---|
| **1** | 39.0 | 17.7 |
| **2** | 38.9 | 17.8 |
| **3** | 38.9 | 17.8 |
| **Average** | 38.9 | 17.8 |

**Table 8.6:** Gas volume measurements by helium porosimeter for sample B.

| Measurement | $V_1\ [cm^3]$ | $V_2\ [cm^3]$ |
|---|---|---|
| **1** | 54 | 20.2 |
| **2** | 54 | 20.4 |
| **3** | 55 | 20.4 |
| **Average** | 54.3 | 20.3 |

**Table 8.7:** Gas volume measurements by helium porosimeter for sample C.

| Measurement | $V_1\ [cm^3]$ | $V_2\ [cm^3]$ |
|---|---|---|
| **1** | 32.0 | 14.2 |
| **2** | 32.0 | 14.2 |
| **3** | 32.0 | 14.2 |
| **Average** | 32.0 | 14.2 |

**Table 8.8:** Gas volume measurements by helium porosimeter for sample D.

| Measurement | $V_1\ [cm^3]$ | $V_2\ [cm^3]$ |
|---|---|---|
| **1** | 32.0 | 14.7 |
| **2** | 32.0 | 14.8 |
| **3** | 32.0 | 14.8 |
| **Average** | 32.0 | 14.8 |